

1 **Inability to switch from ARID1A-BAF to ARID1B-BAF impairs exit from pluripotency and commitment** 2 **towards neural crest differentiation in ARID1B-related neurodevelopmental disorders**

3
4 Luca Pagliaroli¹, Patrizia Porazzi², Alyxandra T. Curtis¹, Harald M.M. Mikkers³, Christian Freund⁴, Lucia
5 Daxinger⁵, Sandra Deliard⁶, Sarah A. Welsh⁶, Connor A. Ott¹, Bruno Calabretta², Gijs W.E. Santen^{*.7}, and
6 Marco Trizzino^{*.1,8}

7
8 * = Co-Senior authors

9 1) Department of Biochemistry and Molecular Biology, Sidney Kimmel Medical College, Thomas Jefferson University,
10 Philadelphia, PA

11 2) Department of Cancer Biology, Sidney Kimmel Medical College, Thomas Jefferson University, Philadelphia, PA

12 3) Department of Cell & Chemical Biology, Leiden University Medical Center, Leiden, The Netherlands

13 4) LUMC hiPSC Hotel, Dept. Anatomy & Embryology, Leiden University Medical Center, Leiden, The Netherlands

14 5) Department of Human Genetics, Leiden University Medical Center (LUMC), Leiden 2300, RC, The Netherlands

15 6) Gene Expression and Regulation Program, The Wistar Institute, Philadelphia, PA

16 7) Department of Clinical Genetics, Leiden University Medical Center, Leiden, The Netherlands

17 8) Corresponding author: Marco Trizzino, Department of Biochemistry and Molecular Biology, Sidney Kimmel
18 Medical College, Thomas Jefferson University, 233 S 10th Street, BLSB 826, Philadelphia, PA, 19104. E-mail:
19 marco.trizzino@jefferson.edu

20 21 **Abstract**

22 The BAF complex modulates genome-wide chromatin accessibility. Specific BAF configurations have been
23 shown to have functional consequences, and subunit switches are essential for cell differentiation.
24 *ARID1B* and its paralog *ARID1A* encode for mutually exclusive BAF subunits. *De novo ARID1B*
25 haploinsufficient mutations cause a neurodevelopmental disorder spectrum, including Coffin-Siris
26 syndrome, which is characterized by neurological and craniofacial features. Here, we reprogrammed
27 *ARID1B*^{+/-} Coffin-Siris patient-derived skin fibroblasts into iPSCs, and investigated cranial neural crest cell
28 (CNCC) differentiation. We discovered a novel BAF configuration (ARID1B-BAF), which includes ARID1B,
29 SMARCA4, and eight additional subunits. This novel version of BAF acts as a gate-keeper which ensures
30 exit from pluripotency and commitment towards neural crest differentiation, by attenuating pluripotency
31 enhancers of the SOX2 network. At the iPSC stage, these enhancers are maintained in active state by an
32 ARID1A-containing BAF. At the onset of differentiation, cells transition from ARID1A-BAF to ARID1B-BAF,
33 eliciting attenuation of SOX2 enhancers and pluripotency exit. Coffin-Siris patient cells fail to perform the
34 ARID1A/ARID1B switch, and maintain ARID1A-BAF at pluripotency enhancers throughout CNCC
35 differentiation. This correlates with aberrant SOX2 binding at pluripotency enhancers, and failure to
36 reposition SOX2 at developmental enhancers. SOX2 dysregulation promotes upregulation of the *NANOG*
37 network, impairing CNCC differentiation. ARID1B-BAF directly modulates *NANOG* expression upon
38 differentiation cues. Intriguingly, the cells with the most prominent molecular phenotype in multiple
39 experimental assays are derived from a patient with a more severe clinical impairment.
40 These findings suggest a direct connection between *ARID1B* mutations, CNCC differentiation, and a
41 pathogenic mechanism for Coffin-Siris syndrome.

42
43 **Keywords:** BAF, ARID1B, Coffin-Siris, pluripotency enhancers, NANOG, SOX2, neural crest, SALL4
44
45
46
47
48
49

50 Introduction

51

52 Cell fate commitment is a complex process that requires timely regulation of developmental genes. This
53 phenomenon is mediated by the concerted activity of transcription factors and chromatin regulators that
54 modulate the interaction between *cis*-regulatory elements (enhancers, promoters) and RNA Polymerase
55 II to elicit gene expression. In this framework, a key role is played by the Brg1/Brm associated factor (BAF)
56 chromatin-remodeling complex. BAF leverages ATP to modulate nucleosome positioning and chromatin
57 accessibility genome-wide¹. Different configurations of BAF, with context specific functions, have been
58 described, and switches between subunits have been reported to be linked to specific developmental
59 stages^{2,3}. All the known BAF configurations require the presence of a subunit containing an AT-rich DNA
60 binding domain (ARID). Namely, in the BAF complex this function is carried out by two mutually exclusive
61 subunits: ARID1A and ARID1B⁴⁻⁶. Previous studies in mouse embryonic stem cells (mESCs) have identified
62 a mESC-specific configuration of BAF which regulates pluripotency and self-renewal of the embryonic
63 stem cells (esBAF)⁴⁻⁶. Importantly, the esBAF exclusively incorporates ARID1A and not ARID1B. One of
64 these studies also identified a non-canonical version of BAF (gBAF) not containing any ARID subunit and
65 also involved in pluripotency maintenance of mouse embryonic stem cells⁴.

66 *De novo* haploinsufficient mutations in the *ARID1B* gene cause a spectrum of neurodevelopmental
67 disorders, ranging from Coffin Siris syndrome to non-syndromic intellectual disability⁷⁻¹². Coffin-Siris
68 syndrome is associated with intellectual disability, specific craniofacial features, growth impairment,
69 feeding difficulties and congenital anomalies such as heart and kidney defects¹³. Although other BAF
70 components may also be mutated in this syndrome, the very large majority of mutations (~75%) are in
71 *ARID1B*^{11,14,15}. In addition to Coffin-Siris, genome-wide sequencing in unselected cohorts of patients with
72 intellectual disability (ID) shows that *ARID1B* is always in the top-5 of causative genes, explaining about
73 1% of all ID cases^{9,16}. Studies in several mouse models were able to recapitulate the neurological
74 phenotypes typical of the *ARID1B*-associated syndromes¹⁷⁻²⁰. Nonetheless, the molecular function of
75 ARID1B in cell fate commitment during human development is still poorly understood.

76 An important feature of *ARID1B* haploinsufficient individuals is represented not only by severe craniofacial
77 abnormalities, but also by defects of the cardiac and digestive systems, often associated with ineffective
78 migration of the cardiac and enteric neural crest¹². Further, *ARID1B* is one of the most commonly mutated
79 genes in neuroblastoma, a pediatric tumor of neural crest origin²¹. For all these reasons, the neural crest
80 differentiation represents one of the most suitable models to study the consequences of *ARID1B*
81 mutations in human development.

82 To investigate the molecular consequences of *ARID1B* haploinsufficient mutations in neural crest
83 differentiation and craniofacial development, we reprogrammed skin fibroblasts of two unrelated
84 *ARID1B*^{-/-} Coffin-Siris patients into induced Pluripotent Stem Cells (iPSCs). Then we used these patient-
85 derived iPSCs to specifically model Cranial Neural Crest Cell (CNCC) differentiation.

86 Thanks to this approach, we report the discovery of a novel BAF configuration, containing ARID1B,
87 SMARCA4 and eight additional subunits (ARID1B-BAF). In line with the evidence that the esBAF and the
88 gBAF do not contain ARID1B⁴⁻⁶, we demonstrate that *ARID1B* mutations do not affect self-renewal and
89 pluripotency of human iPSCs. At this stage, the pluripotency is positively regulated by binding of an
90 ARID1A-containing BAF to pluripotency-associated enhancers of the SOX2 and NANOG networks. On the
91 other hand, we show that ARID1B-BAF plays an important role in lineage specification and exit from
92 pluripotency. In fact, ARID1B-BAF is only transiently active during early stages of CNCC differentiation,
93 where it replaces ARID1A-BAF at the SOX2/NANOG enhancers and elicits their repression. Intriguingly,
94 ARID1B-BAF interacts with SALL4 (Spalt Like Transcription Factor 4), which is a multi-zinc-finger
95 transcription factor essential for lineage commitment in early mammalian development, during which it
96 targets sites with the same binding motifs also recognized by SOX2, OCT4 and NANOG²²⁻²⁵. This
97 transcription factor can act as both activator and repressor and is dispensable for the maintenance of the

98 stem cell pluripotency networks, but it ensures that aberrant gene expression programs are not activated
99 during lineage commitment²³.

100 Importantly, we demonstrate that the *ARID1B*^{-/-} Coffin-Siris cells are unable to switch from ARID1A-BAF
101 to ARID1B-BAF at the onset of the CNCC differentiation, and instead maintain ARID1A-BAF at the
102 pluripotency enhancers throughout the differentiation process. This leads to defective exit from
103 pluripotency and impaired cranial neural crest differentiation. These findings provide evidence for a direct
104 connection between *ARID1B* mutations and a pathogenic mechanism for ARID1B-associated
105 neurodevelopmental syndromes.

106

107

108 **Results**

109

110 **Coffin-Siris patient-derived iPSCs are pluripotent and proliferate normally**

111 To investigate the function of ARID1B in craniofacial development, we obtained skin fibroblasts from two
112 unrelated *ARID1B*^{-/-} Coffin-Siris Syndrome patients (hereafter Patient-19 and Patient-26; Fig. 1a), one
113 male and one female, both carrying previously identified *de novo* *ARID1B* mutations. In detail, Patient-19
114 presented a nonsense mutation (c.3223C>T;p.Arg1075*; Fig. 1b), while Patient-26 had a frameshift
115 mutation (c.2598del;Tyr867Thrfs*47; Fig. 1b)^{10,14}. In both cases, a premature STOP codon was generated
116 (Fig. 1b).

117 The fibroblasts were reprogrammed into iPSCs by the LUMC hiPSC Hotel (Leiden University). The patient-
118 derived iPSCs exhibit regular morphology (Fig. 1c) and express the pluripotency genes, as shown by both
119 immunofluorescence (Fig. 1d; Supplementary Fig. S1a,b) and RT-qPCR (Fig. 1e). Further, the patient-
120 derived iPSCs grow at the same rate as an *ARID1B*^{+/+} control line (Control line-1; Fig. 1f).

121 Importantly, the aberrant STOP codon introduced by the mutations is located either upstream (Patient-
122 26) or inside (Patient-19) the AT-Rich Interactive Domain (ARID) (Fig. 1b), which is required for ARID1B's
123 interaction with chromatin²⁶. Moreover, in both patients, the new STOP codon is localized upstream of
124 the Nuclear Localization Signal (NLS, Fig. 1b), suggesting that the gene product arising from the mutated
125 allele would not be able to reach the nucleus and the chromatin even in the unlikely case that the
126 transcript escaped non-sense mediated mRNA decay²⁷. To test this, we performed cellular fractionation
127 in patient and control iPSCs and conducted an ARID1B western blot on the chromatin fraction with an
128 antibody raised against a peptide in the N-terminus of ARID1B, hence upstream of the mutated regions
129 (sc-32762). Consistent with our hypothesis, the immunoblot on the chromatin fraction shows significantly
130 lower ARID1B protein level in the two patients relative to an *ARID1B*^{+/+} iPSC line (Control line-1;
131 Supplementary Figure S1c). No ARID1B signal was detected in any of the lines in the cytoplasmic fraction
132 (Supplementary Fig S1c).

133 In summary, *ARID1B* haploinsufficient iPSCs are pluripotent, do not exhibit growth defects, but display
134 significantly less chromatin-bound ARID1B.

135

136 **The CNCC differentiation is impaired in Coffin-Siris patient-derived iPSCs**

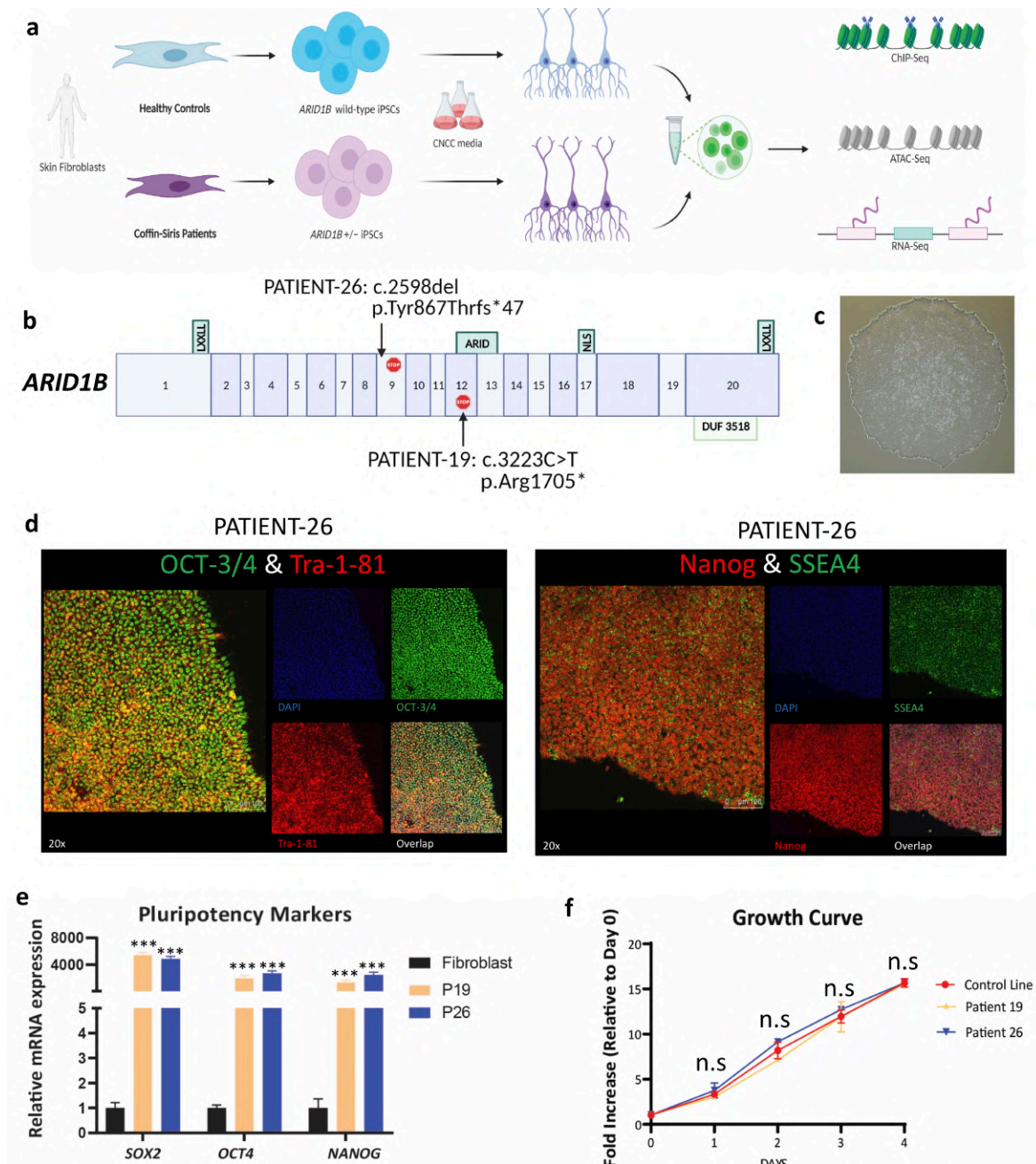
137 We took advantage of a published CNCC differentiation protocol²⁸, and using Control line-1 we obtained
138 fully differentiated Cranial Neural Crest Cells in 14 days (Fig. 2a,b). A time-course western blot conducted
139 during the CNCC differentiation of Control line-1 revealed that ARID1B protein is highly expressed only
140 during the first week of differentiation, peaking between days 5 and 7, after which is markedly
141 downregulated (Fig. 2c).

142

143

144

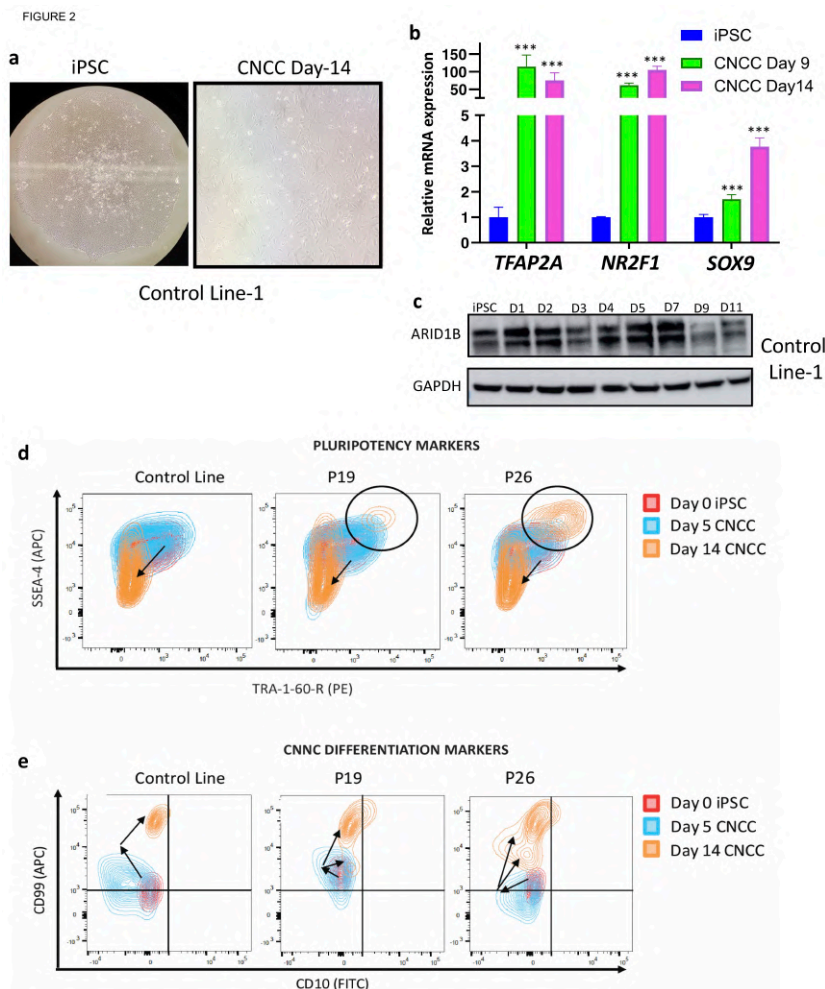
145



146 **Figure 1 – iPSCs derived from Coffin-Siris patients are pluripotent and proliferate normally.** (a) Study
 147 system: iPSCs were derived from skin fibroblasts of two unrelated Coffin-Siris patients. The iPSCs were
 148 used in this study to generate Cranial Neural Crest Cells (CNCCs) and perform genomic experiments to
 149 investigate the effect of *ARID1B* mutations. (b) Graphical illustration of the *ARID1B* haploinsufficient
 150 mutations affecting the two studied patients. The numbers in the gene model refer to *ARID1B*'s isoform
 151 NM_020732.3. (c) Colony of iPSCs derived from Patient-19 showing typical iPSC morphology. (d, e)
 152 Immunofluorescence and rt-qPCR quantifying the expression of the key pluripotency markers in iPSCs
 153 derived from Patient-26. (f) Growth curve comparing an *ARID1B*-wt Control iPSC Line with the two patient
 154 lines. The patient cells do not exhibit growth impairment.

155
 156

157 Next, we induced the differentiation in the two Coffin-Siris lines and the Control line-1 together, and used
 158 flow cytometry to measure multiple pluripotency (SSEA-4, TRA-1-60-R) and CNCC (CD10, CD99) surface
 159 markers. The cells were sampled at day-zero (iPSC stage), day-5 (mid-point), and day-14 (end of
 160 differentiation). Notably, the differentiation was impaired in both patient lines. In fact, in both lines we
 161 identified a sizable cell population still double-positive for the pluripotency surface markers even after 14
 162 days (Fig. 2d). This pluripotent population comprised 4.36% and 19.5% of the cells in the two patient
 163 lines, respectively (Fig. 2d). In line with this, relative to the control line, a large fraction of the patient cells
 164 showed significantly lower expression of the CNCC surface markers even after 14 days of differentiation
 165 relative to the control line (Fig. 2e). Together, our data suggest that while *ARID1B* is dispensable for
 166 pluripotency, haploinsufficiency of this gene is enough to severely impair differentiation into CNCCs.



196 **Figure 2 – CNCC differentiation is impaired in the patient cells. (a, b)** CNCC differentiation was optimized
 197 using an *ARID1B*-wt Control Line. After 14 days, the cells exhibited the classic CNCC morphology and
 198 expressed the CNCC markers. **(c)** Time-course immunoblot conducted using Control Line-1 during CNCC
 199 differentiation shows that *ARID1B* is active in the first 7 days of the differentiation, with a peak of activity
 200 between day-5 and day-7. The *ARID1B* protein level strongly decreases after day-7. **(d, e)** Flowcytometry
 201 quantifying expression of surface markers for pluripotency and CNCC differentiation in control line-1 and
 202 in the two patient lines. A large cell population is still pluripotent in both patients after 14 days (d). The
 203 patient lines also show reduced expression of CNCC surface markers after 14 days of differentiation
 204 relative to an *ARID1B*-wt Control Line at the same time point (e).

205 **Chromatin accessibility is dysregulated in the differentiating patient cells**

206 We used Next-Generation Sequencing to investigate why *ARID1B* haploinsufficient Coffin-Siris iPSCs did
207 not successfully differentiate into CNCCs. Given that ARID1B protein levels in control cells reach a peak
208 between days 5 and 7, we selected day-5 as a time-point to collect the genomic data. The experiments
209 were conducted with two biological replicates per condition (two control lines, two patient lines). For
210 each condition, a male and a female were included to avoid sex-specific confounding effects. Technical
211 replicates were also performed for each biological replicate. To avoid batch effects, all the biological
212 replicates and conditions were processed together.

213 Since ARID1B is a component of the BAF chromatin-remodeling complex, we profiled chromatin
214 accessibility with ATAC-seq. Overall, we detected 29,758 ATAC-seq peaks replicated across all replicates
215 and all conditions (patients and controls; FDR <0.05; Fig. 3a). Conversely, 5,540 peaks were specific to the
216 patients (i.e. replicated in all the patient replicates and not detected in any of the controls; hereafter
217 patient-specific ATAC-seq regions; Fig. 3a,b; Supplementary File S1). Finally, only 578 peaks were specific
218 to the controls (hereafter control-specific ATAC-seq regions; Fig. 3a,c; Supplementary File S1).

219 We therefore focused on the 5,540 patient-specific ATAC-seq regions because they represented 91%
220 (5,540/6,118) of all regions with differential chromatin accessibility between patients and controls.
221 ARID1B ChIP-seq performed in the Control Line-1 at the day-5 shows ARID1B binding in all of these regions
222 (Fig. 3d). This suggests that the chromatin accessibility in the 5,540 patient-specific ATAC-seq regions may
223 be directly regulated by ARID1B-BAF. In line with this, ARID1B ChIP-seq performed on all four lines at day-
224 5 of differentiation confirmed that the 5,540 patient-specific ATAC-seq regions are similarly bound by
225 ARID1B in both control lines, while the binding is almost entirely lost in both patient lines (Supplementary
226 Fig. S2a).

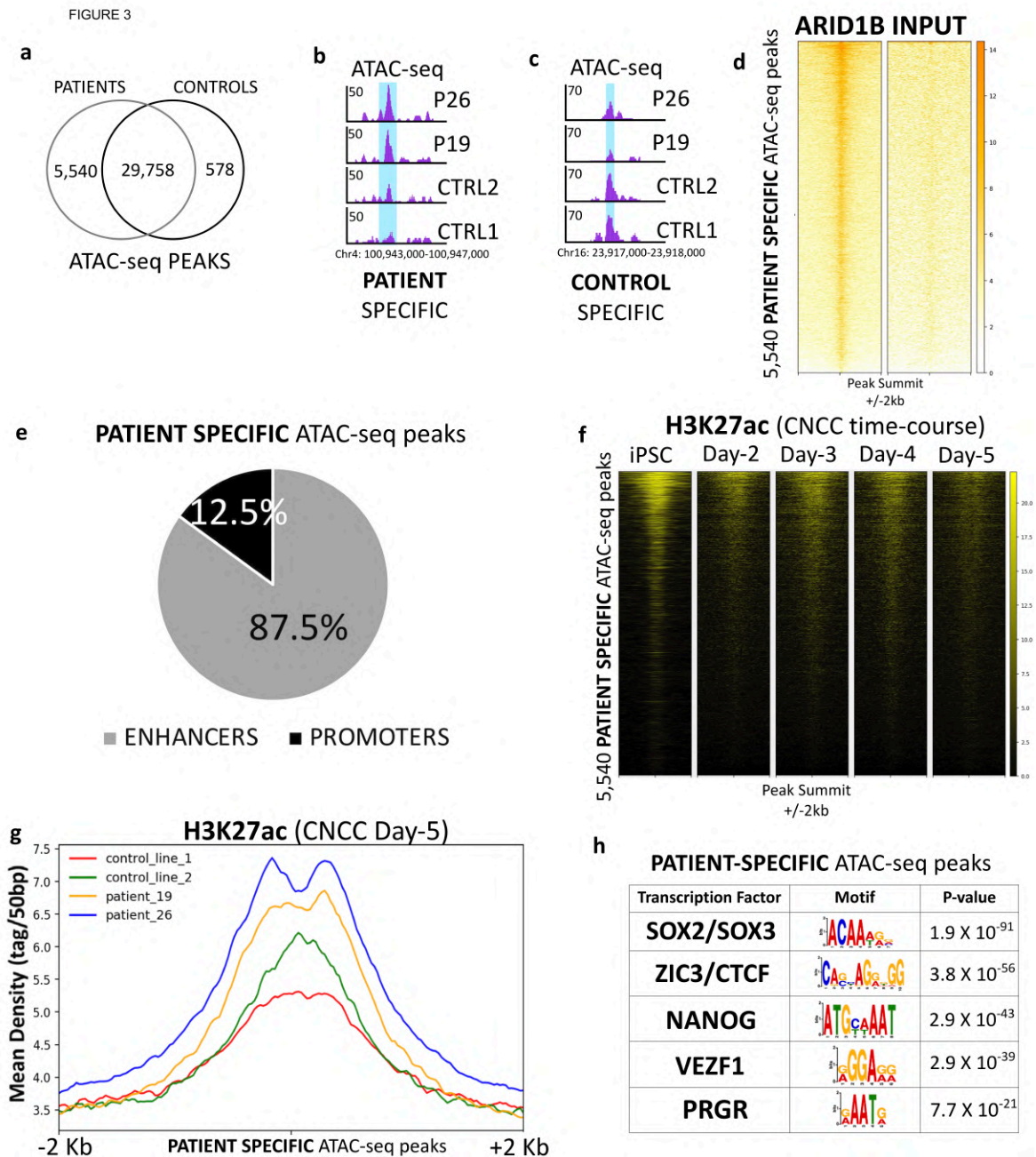
227

228 **The ARID1B-BAF attenuates thousands of enhancers at the onset of CNCC differentiation**

229 To determine the genomic nature of these regions, we associated a gene to each region based on the
230 distance from the nearest Transcription Start Site (TSS). Overall, 87.5% of the ARID1B ChIP-seq peaks
231 were located >10 Kb from the nearest TSS and may represent putative enhancers, while the remaining
232 12.5% are likely promoters (Fig. 3e). ChIP-seq time-course for H3K27ac in Control Line-1 revealed that
233 many of these regulatory regions are enriched for H3K27ac in iPSCs, while their regulatory activity
234 progressively decreases upon differentiation cues, and by day-5 very little H3K27ac signal is detectable
235 (Fig. 3f). Notably, the gradual decrease in H3K27ac mirrors the steady increase in ARID1B expression
236 detected during the early stages of CNCC differentiation (Fig. 2c). Consistently, the differentiating CNCCs
237 of both patients have significantly higher levels of H3K27ac in these regions relative to the two control
238 lines at the day-5 (Wilcoxon's Rank Sum Test $p < 2.2 \times 10^{-16}$ in all the patient vs control pairwise
239 comparisons; Fig. 3g).

240 Based on the high H3K27ac signal that the 5,540 patient-specific regions display at the iPSC stage (Fig. 3f),
241 we surmised that these sites could represent cis-regulatory elements important for pluripotency. In line
242 with this hypothesis, DNA-motif analysis on the 5,540 regions revealed that they are enriched for the
243 binding sites of multiple pluripotency factors, including SOX2 and NANOG (Fig. 3h; Supplementary File S2).
244 Next, we wanted to ensure that the molecular phenotypes observed so far were directly caused by the
245 *ARID1B* mutations, and not by co-occurring mutations in other genes coincidentally shared by both
246 (unrelated) patients. Hence, we employed shRNAs to knock-down ARID1B in the Control Line-1. We were
247 able to obtain a partial knock-down of ARID1B at the iPSC stage (shRNA-1; Supplementary Fig. 2b), which
248 represented a suitable model for *ARID1B* haploinsufficiency. We differentiated the ARID1B-KD iPSCs
249 towards CNCC and again collected the cells at the day-5, and performed ATAC-seq and ChIP-seq for
250 H3K27ac. Notably, both sequencing experiments perfectly recapitulated what we previously observed in
251 the patient lines.

252



253 **Figure 3 – Chromatin remodeling at pluripotency enhancers is dysregulated in the patient cells.** (a) At
 254 CNCC day-5, 29,578 ATAC-seq peaks are shared between patient and control lines. 5,540 peaks are specific
 255 of the patients. 578 peaks are specific of the control lines. (b) UCSC Genome Browser example of a
 256 PATIENT-SPECIFIC ATAC-seq peak. (c) UCSC Genome Browser example of a CONTROL-SPECIFIC ATAC-seq
 257 peak. (d) ARID1B ChIP-seq heatmaps (Control Line-1; CNCC Day-5) show ARID1B binding at nearly all of
 258 the PATIENT-SPECIFIC ATAC-seq peaks. The input (collected at CNCC Day-5) was used as a control (e)
 259 87.5% of the PATIENT-SPECIFIC ATAC-seq peaks are located > 1kb from a TSS. (f) Heatmaps of H3K27ac
 260 ChIP-seq time-course at the 5,540 PATIENT-SPECIFIC ATAC-seq peaks (Control Line-1). (g) H3K27ac ChIP-
 261 seq average profiles centered on the PATIENT-SPECIFIC ATAC-seq regions (CNCC Day-5). (h) Motif analysis
 262 at the PATIENT-SPECIFIC ATAC-seq regions revealed enrichment for the binding motif of multiple
 263 pluripotency factors.

264 Namely, upon ARID1B-KD, we detected significantly increased chromatin accessibility and H3K27ac signal
265 in the 5,540 patients-specific regions relative to the same iPSC line transduced with a control shRNA
266 (Wilcoxon's Rank Sum Test $p < 2.2 \times 10^{-16}$; Supplementary Fig. S2c,d).

267 Together, these data indicate that ARID1B-BAF modulates the chromatin accessibility of a specific set of
268 ~4,900 pluripotency enhancers and ~600 promoters that are highly active at the iPSC stage, moderately
269 active at the CNCC differentiation onset, and inactive by day-5 (Fig. 3f). We find that the attenuation of
270 these cis-regulatory elements is impaired in the *ARID1B* haploinsufficient cells, which likely hampers the
271 entire differentiation process towards CNCCs.

272

273

274 **"Pluripotency" and "Exit from Pluripotency" genes are dysregulated in the differentiating patient cells**

275 Impaired attenuation of ~4,900 pluripotency-relevant enhancers and ~600 promoters could have a
276 profound effect on gene expression levels. Indeed, RNA-seq conducted on the four lines at CNCC Day-5
277 identified 2,356 differentially expressed genes, 1,685 of which were downregulated, and 671 upregulated
278 (FDR <5%; Fig. 4a). As expected, *ARID1B* was one of the top downregulated genes in patient CNCCs at the
279 day-5 (Fig. 4a). In stark contrast, only 54 genes were identified as differentially expressed when we
280 performed RNA-seq at the iPSC stage (FDR <5%). This suggests that ARID1B has an important function
281 upon lineage commitment, again mirroring the progressive increase in the ARID1B protein level observed
282 during early differentiation (Fig. 2c). These findings are consistent with previous studies that
283 demonstrated that the mESC BAF complexes (esBAF, gBAF) do not include ARID1B⁴⁻⁶.

284 Notably, 598/2,356 (25.4%) of the genes differentially expressed at CNCC day-5 also represented the
285 nearest gene to one of the 5,540 pluripotency enhancers and promoters aberrantly active in the Coffin-
286 Siris patient cells at the same time point (Fisher's Exact Test $p < 0.0001$; Supplementary File S3). These
287 results suggest that over a quarter of the differentially expressed genes are under the direct control of
288 ARID1B-BAF throughout modulation of the chromatin accessibility at the associated enhancers and
289 promoters. As expected, when we compared these 598 genes against the entire set of differentially
290 expressed genes, we found that the 598 genes exhibit enrichment for genes upregulated in patients
291 (Fisher's Exact Test $p < 0.0001$), likely determined by increased activity in the associated enhancers and
292 promoters.

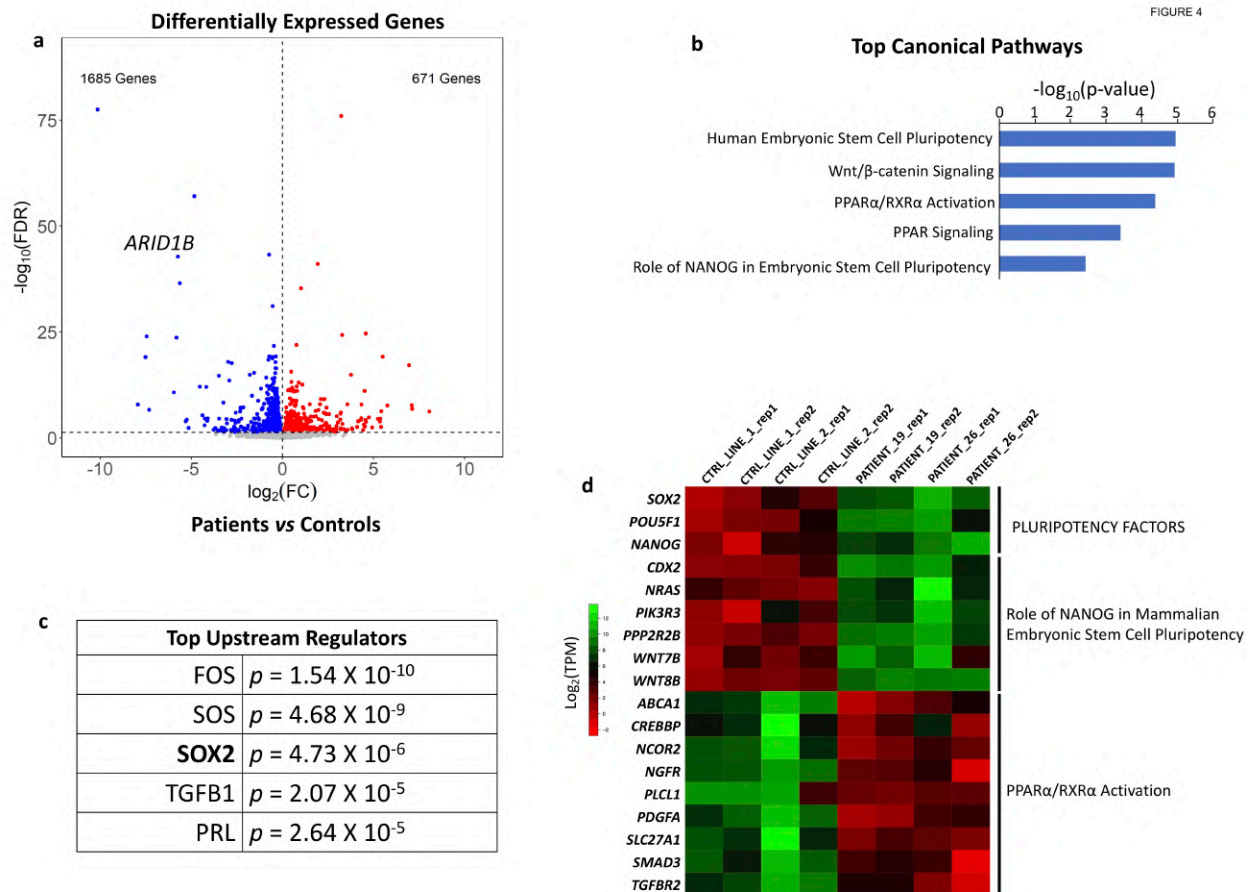
293 Ingenuity Pathway Analysis on the 598 genes identified five of the top canonical pathways as associated
294 with either pluripotency or exit from pluripotency (Fig. 4b; Supplementary File S4). Wnt- β catenin
295 signaling pathway was also found as enriched. An association between ARID1B and this specific pathway
296 was suggested in recent studies^{29,30}.

297 In accordance with the ATAC-seq data, SOX2 was detected among the top upstream regulators (Fig. 4c),
298 and three of the most important pluripotency factors, and specifically *NANOG*, *SOX2* and *POU5F1* (OCT4),
299 were found as still highly expressed in the patient lines at the day-5 (Fig. 4d).

300 Both the "*Role in NANOG in Mammalian Embryonic Stem Cell Pluripotency*" pathway and the
301 "*PPAR α /RXR α Activation*" pathway were enriched in the 598 genes (Fig. 4b). Namely, the genes belonging
302 to the former pathway were all upregulated, while the genes belonging to the latter were downregulated
303 (Fig. 4d). These two pathways caught our attention because they are thought to antagonize each other.
304 More specifically, NANOG blocks the differentiation of pluripotent cells and establishes the pluripotent
305 state during somatic cell reprogramming. On the other hand, the PPAR α /RXR α pathway is activated at
306 the onset of differentiation to promote exit from pluripotency³¹. The activation of PPAR α /RXR α elicits the
307 repression of the *NANOG* network to allow efficient exit from the undifferentiated stage³¹⁻³³. Consistent
308 with this, PPAR α -inhibitors have been employed to enhance and improve iPSC reprogramming³¹.

309 Taken together, our RNA-seq data suggest that the differentiating *ARID1B*^{+/-} patient lines exhibit a
310 persistent upregulation of multiple pluripotency factors and associated gene networks, along with

311 downregulation of genes responsible for exit from pluripotency, which impairs the differentiation
 312 program to CNCC.
 313

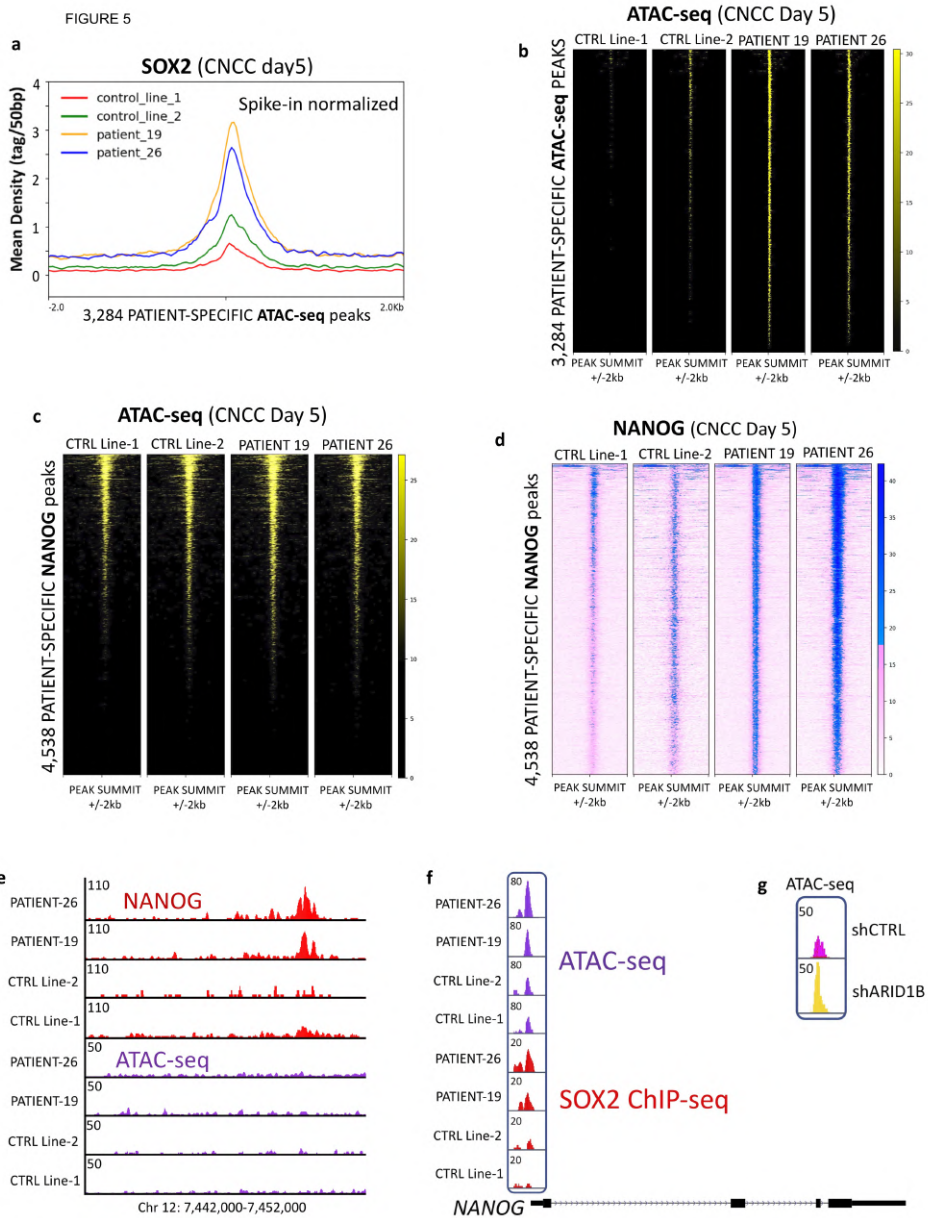


314
 315
 316 **Figure 4 – “Pluripotency” and “Exit from Pluripotency” genes are dysregulated in differentiating patient**
 317 **CNCCs. (a)** RNA-seq volcano plot shows the differentially expressed genes between patient and control
 318 lines at CNCC Day-5. *ARID1B* is one of the top downregulated genes. **(b)** Top canonical pathways (IPA
 319 analysis) enriched in the set of 598 differentially expressed genes that also represent the closest gene to
 320 a PATIENT-SPECIFIC ATAC-seq peak. **(c)** Top upstream regulators (IPA analysis) enriched in the same set
 321 of 598 genes used for panel b. **(d)** RNA-seq heatmap displaying expression patterns at CNCC Day-5 for
 322 pluripotency genes, for genes of the NANOG network, and for genes associated to exit from pluripotency
 323 (PPAR α /RXR α activation pathway).

324
 325
 326 **Aberrant SOX2 and NANOG activity in the *ARID1B* haploinsufficient patient cells**
 327 Our experiments indicate that the *ARID1B* haploinsufficient cells fail to attenuate thousands of
 328 pluripotency enhancers and promoters enriched for SOX2 and NANOG binding sites (Fig. 3a–h). Further,
 329 at day-5 of CNCC differentiation, the expression of SOX2 and NANOG is significantly higher in the patient
 330 derived cells than in the controls, and the gene regulatory networks associated with these pluripotency
 331 factors are also upregulated (Fig. 4b–d).

332 Given these results, we set out to investigate the binding profile of SOX2 and NANOG in patient and
333 control lines by ChIP-seq at CNCC day-5. Our spike-in normalized SOX2 ChIP-seq revealed that 3,284/5,540
334 (59.7%) patient-specific ATAC-seq peaks are characterized by significantly higher SOX2 binding in patients
335 relative to the control lines. In line with this, the chromatin at these regions is accessible in the patient
336 lines but not in the control lines (Fig. 5b). SOX2 is a pioneer factor that is able to bind condensed
337 nucleosomes to open the chromatin for the binding of other factors³⁴. As demonstrated by previous
338 studies in mouse in embryonic stem cells SOX2 and other pluripotency pioneer factors (e.g. OCT4) require
339 the BAF complex to perform their pioneer activity^{6,34,35}. Our findings indicate that in control conditions
340 ARID1B-BAF complex likely antagonizes the cooperation between other BAF configurations and SOX2,
341 counter-acting the pioneer activity of the latter as soon as the cell differentiation is induced. Further, we
342 identified an additional set of 497 SOX2 peaks specific of the patient lines, which did not exhibit changes
343 in chromatin accessibility. Moreover, we also identified 1,146 SOX2 peaks exclusive of the control lines
344 (Supplementary File S5). Importantly, these control-specific SOX2 peaks were located in proximity to
345 genes associated with neural crest differentiation, including *TFAP2A*, *PAX6*, *PAX7*, *WNT4*, *ENO1*, *C8B*, and
346 *SERBP1* among others. These findings are consistent with two recent studies which suggested that SOX2-
347 chromatin interactions are rewired upon differentiation cues^{36,37}. Such rewiring appears impaired in
348 *ARID1B*-haploinsufficient cells, which aberrantly maintain SOX2 at the pluripotency-associated enhancers,
349 and at the same time fail to reposition this transcription factor at the developmental enhancers.
350 Next, we profiled NANOG at day-5 of differentiation. For this transcription factor, the spike-in normalized
351 ChIP-seq revealed 4,538 peaks unique to the patients (Supplementary File S6). However, in this case, only
352 219 (4.8%) of the patient-specific NANOG peaks overlapped a patient-specific ATAC-seq peak. We thus
353 interrogated our ATAC-seq data to determine the state of chromatin accessibility at the 4,538 patient-
354 specific NANOG peaks, and overall found no significant changes in accessibility in these regions between
355 the patients and the control lines (Fig. 5c). Notably, nearly a quarter of the patient-specific NANOG peaks
356 were found in regions of repressed chromatin (Fig. 5c,e), consistent with recent studies which suggested
357 that NANOG can bind repressed chromatin like other pioneer pluripotency factors^{38,39}.
358 Despite no changes in chromatin accessibility, the NANOG ChIP-seq signal at the 4,538 patient-specific
359 NANOG peaks was significantly higher in the patient than in the control lines (Wilcoxon's Rank Sum Test
360 $p < 2.2 \times 10^{-16}$ in all the patient vs control pairwise comparisons; Fig. 5d,e). We hypothesized that the
361 increased NANOG binding detected in the patients' cells (Fig. 5d) could reflect increased *NANOG*
362 expression (Fig. 4d). In fact, several elegant studies in embryonic stem cells have demonstrated that the
363 downregulation of *NANOG* gene expression marks the transition from naïve to primed state⁴⁰⁻⁴².
364 Importantly, it has been shown that *NANOG* expression is modulated by SOX2, which binds a cis-
365 regulatory element in the promoter region of *NANOG*^{43,44}. Thus, we examined this cis-regulatory element
366 in detail. As expected, at day-5 of CNCC differentiation, the chromatin accessibility at the promoter-
367 proximal element is significantly higher in the two patient lines than in the two controls (Student's T-Test
368 $p=0.0065$; Fig. 5f). Accordingly, increased chromatin accessibility correlates with increased SOX2 binding
369 on the cis-regulatory element (Fig. 5f), perhaps explaining the higher *NANOG* gene expression reported in
370 patients at CNCC day-5. Lastly, our shRNA experiments also replicated these findings, demonstrating that
371 the knock-down of ARID1B in the Control line-1 line correlates with a sizeable increase in accessibility at
372 the *NANOG* cis-regulatory element (Fig. 5g), thus suggesting that ARID1B-BAF directly modulates *NANOG*
373 expression dosage at the onset of differentiation.
374 In sum, the *ARID1B* haploinsufficient lines exhibit persistent activity of two key pluripotency factors (SOX2,
375 NANOG) in the early stages of CNCC differentiation. The aberrant activity of SOX2 and NANOG leads to
376 impaired lineage commitment and inefficient CNCC differentiation.

377
378
379



380
381
382
383
384
385
386
387
388
389
390
391
392
393

Figure 5 – Aberrant SOX2 and NANOG activity in the patient cells at CNCC Day-5. (a) SOX2 ChIP-seq average profile for 3,284 patient-specific ATAC-seq peaks showing patient-specific SOX2 signal (spike-in normalized; CNCC Day-5). (b) ATAC-seq heatmaps at the 3,284 peaks shown in Fig. 5a reveal that these regions display increased chromatin accessibility in the patients relative to the two control lines. (c) ATAC-seq heatmaps at 4,538 patient-specific NANOG peaks display no changes in accessibility between patient and control lines. (d) NANOG ChIP-seq heatmaps at 4,538 patient-specific NANOG peaks (spike-in normalized; CNCC Day-5). (e) Example of patient-specific NANOG peak in a region with no chromatin accessibility (CNCC Day-5). (f) At CNCC Day-5, a cis-regulatory element in the promoter region of *NANOG* is more accessible in the patients than in the control lines. The same element also displays higher SOX2 binding in the patients than in the controls. (g) Knock-down of ARID1B from Control Line-1 also elicits an increase in chromatin accessibility at the cis-regulatory element in the promoter region of *NANOG* (CNCC Day-5).

394 **A switch from ARID1A-BAF to ARID1B-BAF is necessary for exit from pluripotency**

395 We wanted to elucidate how the BAF complex compensates for *ARID1B* haploinsufficiency. As mentioned
396 earlier, ARID1A and ARID1B represent the only two subunits of the BAF harboring an ARID domain, which
397 is leveraged by the complex to interact with the chromatin²⁶. A third ARID subunit (ARID2) is exclusive of
398 a different configuration of the complex (pBAF). *ARID2* mutations have shown to cause a
399 neurodevelopmental disorder that does not fully fit the Coffin-Siris syndrome phenotype, although there
400 is some overlap⁴⁵. Compensation mechanisms between ARID1A and ARID1B were recently demonstrated
401 in ovarian cancer⁴⁶. We hence hypothesized that the *ARID1B* haploinsufficient patient cells may
402 compensate for partial loss of ARID1B with ARID1A. To test this, we first assessed ARID1A protein levels
403 in *ARID1B*-wt cells during the course of CNCC differentiation and found that ARID1A exhibits a pattern of
404 activity complementary to ARID1B (Fig. 6a). In agreement with the specific composition of the esBAF,
405 which requires ARID1A^{5,6}, the human iPSCs show high ARID1A protein level and relatively low ARID1B (Fig.
406 6a). On the other hand, on day-1 of CNCC differentiation ARID1B is immediately upregulated while the
407 ARID1A protein is completely repressed and is no longer detectable (Fig. 6a). ARID1B remains the only
408 active ARID1 subunit between day-1 and day-7 (Fig. 6a). Finally, after day-7, ARID1B is abruptly
409 downregulated while high ARID1A protein level is reprinted (Fig. 6a). Together, these data suggest
410 that in *ARID1B*-wt conditions the differentiating CNCCs perform multiple switches between ARID1A and
411 ARID1B, the most critical likely taking place as soon as the differentiation is induced. We previously
412 identified the time-frame between days 5 and 7 as the peak of ARID1B expression during CNCC
413 differentiation (Figs. 2c and 6a). In this time-frame ARID1A is not active in wild-type conditions (Fig. 6a).
414 Nonetheless, the differentiating cells from both patients present high ARID1A protein levels at this time
415 point, as opposed to almost no detectable protein in the Control line (Fig. 6b). This confirms that patient
416 cells compensate for the partial loss of ARID1B by maintaining high ARID1A levels throughout the
417 differentiation process. A recent study conducted on liver cells demonstrated that ARID1A-containing
418 BAF and ARID1B-containing BAF may have antagonistic function in the transcriptional regulation of
419 specific genes, with ARID1B acting prevalently as a repressor of enhancer elements, as opposed to the
420 ARID1A, which mostly behaves as an activator⁴⁷. Hence, we hypothesized that the aberrantly high ARID1A
421 protein levels detected in the patient-derived cells during CNCC differentiation might underlie the long-
422 lasting activity of the pluripotency enhancers. Consistently, ARID1A-ChIP followed by qPCR revealed that
423 the pluripotency enhancers are bound by ARID1A at the iPSC stage in both the control and the patient
424 lines at comparable levels (Fig. 6c; *p-values* in Supplementary File S7). On the other hand, at the day-5
425 ARID1A binding is completely lost in the control lines – which have meanwhile gained ARID1B at the same
426 sites (Fig. 3d) – while it is maintained in both patient lines (Fig. 6c; *p-values* in Supplementary File S7).
427 To confirm genome-wide that all the 5,540 pluripotency enhancers are bound by ARID1A in the patients,
428 we performed ARID1A ChIP-seq in the patient lines at day-5 of CNCC differentiation. In agreement with
429 the ChIP-qPCR data, the ChIP-seq demonstrated that all the 5,540 pluripotency elements are bound by
430 ARID1A in both patients at CNCC Day-5 (Fig. 6d). The persistent binding of the ARID1A-BAF at the
431 pluripotency enhancers could perhaps explain why the patient cells do not efficiently repress these
432 regions at the onset of the neural crest differentiation.

433 434 **The ARID1B-BAF complex exclusively incorporates SMARCA4 as ATPase subunit**

435 Finally, we designed a set of experiments to shed light on the composition of the ARID1B-BAF at the day-
436 5 of CNCC differentiation. Thus, we performed immunoprecipitation of endogenous ARID1B followed by
437 mass-spectrometry (IP-MS) in Control Line-1. With this approach, ARID1B coeluted with a total of 9
438 additional BAF subunits (Fig. 6d). In mammals, the BAF complexes can incorporate two widely
439 interchangeable and mutually exclusive ATPase subunits (i.e. SMARCA2, and SMARCA4). Remarkably,
440 SMARCA4 was the only ATPase subunit identified as coeluting with ARID1B in our IP-MS, while zero
441 peptides of SMARCA2 were detected (Fig. 6e).

442
443
444
445
446
447
448
449
450
451
452
453
454
455
456
457
458
459
460
461
462
463
464
465
466
467
468
469
470
471
472
473
474
475
476
477
478
479
480
481
482
483
484
485
486
487
488
489

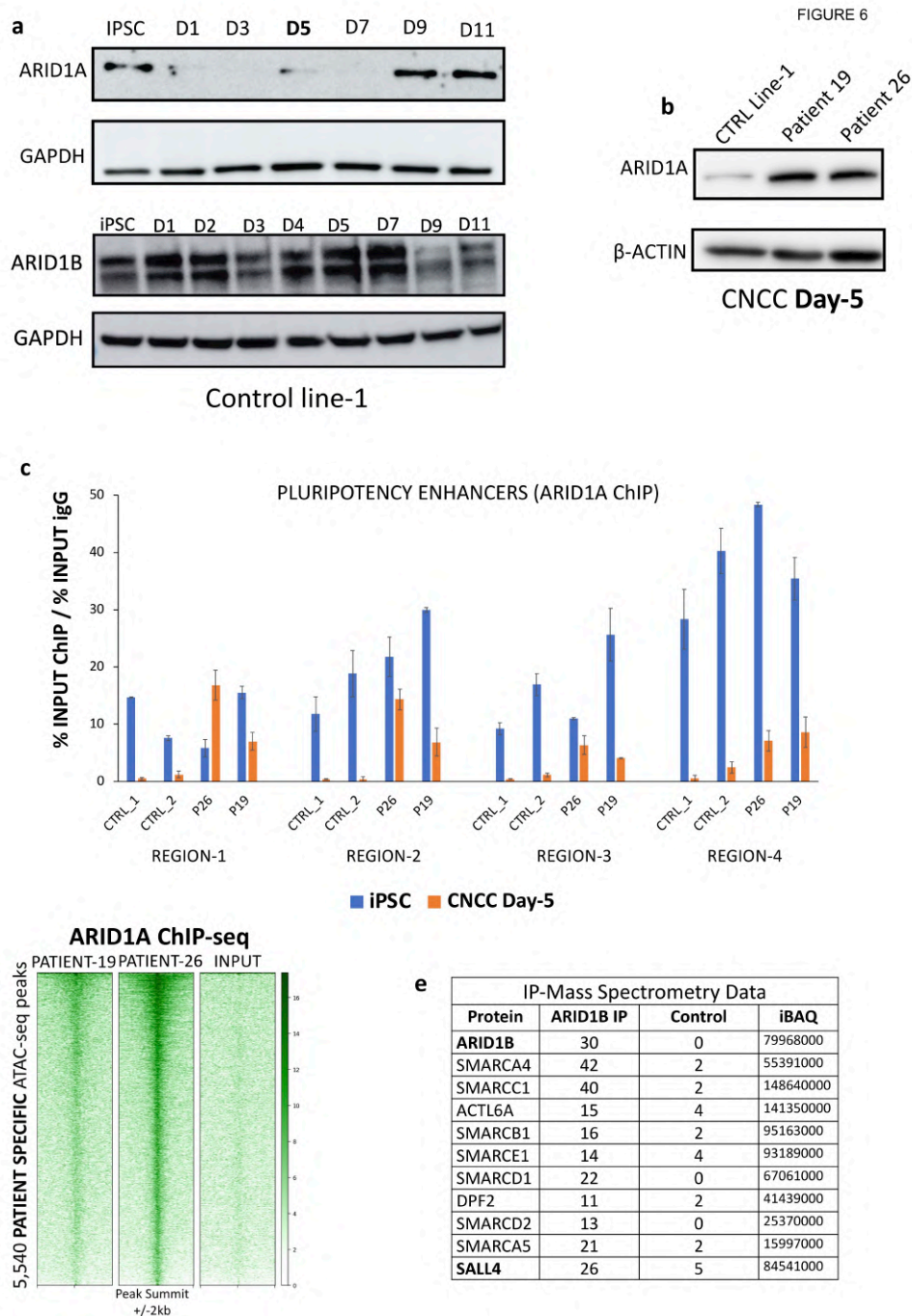


Figure 6 – A switch between ARID1A-BAF and ARID1B-BAF is required for a successful exit from pluripotency. (a) Time-course immunoblot conducted using Control Line-1 during CNCC differentiation shows that ARID1A is active at the iPSC stage, and abruptly downregulated at day-1 of differentiation. ARID1A protein level is upregulated again after day-7, mirroring ARID1B’s downregulation at the same time point (ARID1B blot duplicated here from Fig. 2c for convenience). **(b)** ARID1A immunoblot: both patient lines display aberrantly high ARID1A’s protein level at CNCC Day-5. **(c)** ChIP-qPCR of ARID1A at select pluripotency enhancers: at the iPSC stage the enhancers are bound by ARID1A comparably in both patient and control lines. At CNCC Day-5, the binding is completely lost in the patients while it is at least partially maintained in the patient lines. Coordinates and p-values (T-Test) in Supplementary File S7. **(d)**

490 ChIP-seq for ARID1A in the two patient lines at CNCC Day-5. Heatmaps are centered on the 5,540
491 pluripotency enhancers. Input collected at CNCC Day-5 was used as a control. (e) Table displaying all the
492 BAF subunits (plus SALL4) that coeluted with ARID1B in the IP-MS performed at Day-5 of CNCC5
493 differentiation in Control Line-1. Values represent unique peptide numbers. iBAQ values are shown in
494 last column.

495
496

497 This suggests that ARID1B-BAF selectively incorporates only SMARCA4 as a catalytic subunit, while it does
498 not tolerate the incorporation of SMARCA2.

499 In summary, the IP-MS allowed us to characterize a novel configuration of the BAF complex (ARID1B-BAF),
500 which is active during early stages of cranial neural crest differentiation and includes ARID1B, SMARCA4,
501 and eight additional BAF subunits (Fig. 6e). Intriguingly, the transcription factor SALL4 also coeluted with
502 ARID1B, suggesting a possible interaction with the complex, which was further supported by co-IP
503 (Supplementary Fig. 3). Like ARID1B, SALL4 is also dispensable for the maintenance of the pluripotency
504 networks, while it is essential for lineage commitment in early mammalian development, during which it
505 targets sites with binding motifs also recognized by SOX2, OCT4 and NANOG²²⁻²⁵. SALL4 was previously
506 shown to interact with the NuRD repressive complex²³, while interactions with BAF have been largely
507 unexplored. It was recently demonstrated that this transcription factor has affinity for AT-rich regions⁴⁸,
508 thus providing further support to the ARID1B-SALL4 interaction. *SALL4* mutations are also associated with
509 developmental syndromes, including Okhiro syndrome, Holt-Oram syndrome, and Townes-Brocks
510 Syndrome⁴⁹. Notably, the *SALL4* gene is downregulated in the Coffin-Siris patients at CNCC day-5 but not
511 in undifferentiated iPSCs, suggesting a possible feedback mechanism between *ARID1B* and *SALL4* during
512 lineage commitment. Future studies will be necessary to support the speculation that SALL4 serves as an
513 mediator for ARID1B-BAF recruitment at the pluripotency enhancers.

514

515 Discussion

516 ARID1B is a member of the evolutionarily conserved SWI/SNF (BAF) chromatin remodeler^{26,50}. *De novo*
517 haploinsufficient mutations in the *ARID1B* gene cause severe neurodevelopmental disorders which affect
518 both physical and cognitive development.

519 In this study, we investigated the Coffin-Siris-associated *ARID1B* mutations in the context of craniofacial
520 development and report the discovery of a novel function of the BAF complex: attenuation of the gene
521 expression program associated with pluripotency maintenance upon differentiation cues. We found that
522 this repressive function is performed at pluripotency enhancers and promoters by a specific and novel
523 BAF complex configuration (ARID1B-BAF), which is composed of 10 subunits, with the enzymatic activity
524 seemingly carried out exclusively by SMARCA4.

525 As a consequence of the *ARID1B* mutations, the Coffin-Siris patient cells fail to repress the pluripotency
526 elements. This elicits aberrant SOX2 activity genome-wide, which in turn leads to the upregulation of
527 multiple pluripotency genes, including *NANOG* and its associated gene network, and to the
528 downregulation of the genes responsible for coordinating the exit from pluripotency
529 (*PPAR α* /*RXR α* pathway). We demonstrate that these pluripotency enhancers are normally maintained in
530 an active state by ARID1A-BAF at the iPSC stage, and subsequently repressed by the ARID1B-BAF at the
531 onset of cranial neural crest differentiation.

532 A switch between ARID1A-BAF and ARID1B-BAF upon differentiation cues is hence necessary for
533 commitment towards the neural crest lineage.

534 Other studies have previously suggested that switches between SWI/SNF subunits play important roles in
535 cell fate determination. For example, a switch between the two catalytic subunits SMARCA4 and
536 SMARCA2 mediates the activation of human IFN γ -activated genes⁵¹. Similarly, a gain of the subunit
537 BAF53a in the neuron-specific BAF (nBAF) is required to control cell cycle exit in the developing neurons^{2,3}.

538 With our study, we discovered a novel switch between BAF subunits (ARID1A/ARID1B), critical for the exit
539 from pluripotency. Importantly, a balance between pro-self-renewal and pro-differentiation signals is
540 pivotal for the determination of stem cell fate⁵². We demonstrate that such balance is lost in Coffin-Siris
541 patients, whose cells are unable to perform the ARID1A/ARID1B switch at the pluripotency enhancers at
542 the onset of differentiation. This switch is essential to successfully complete the cranial neural crest
543 differentiation.

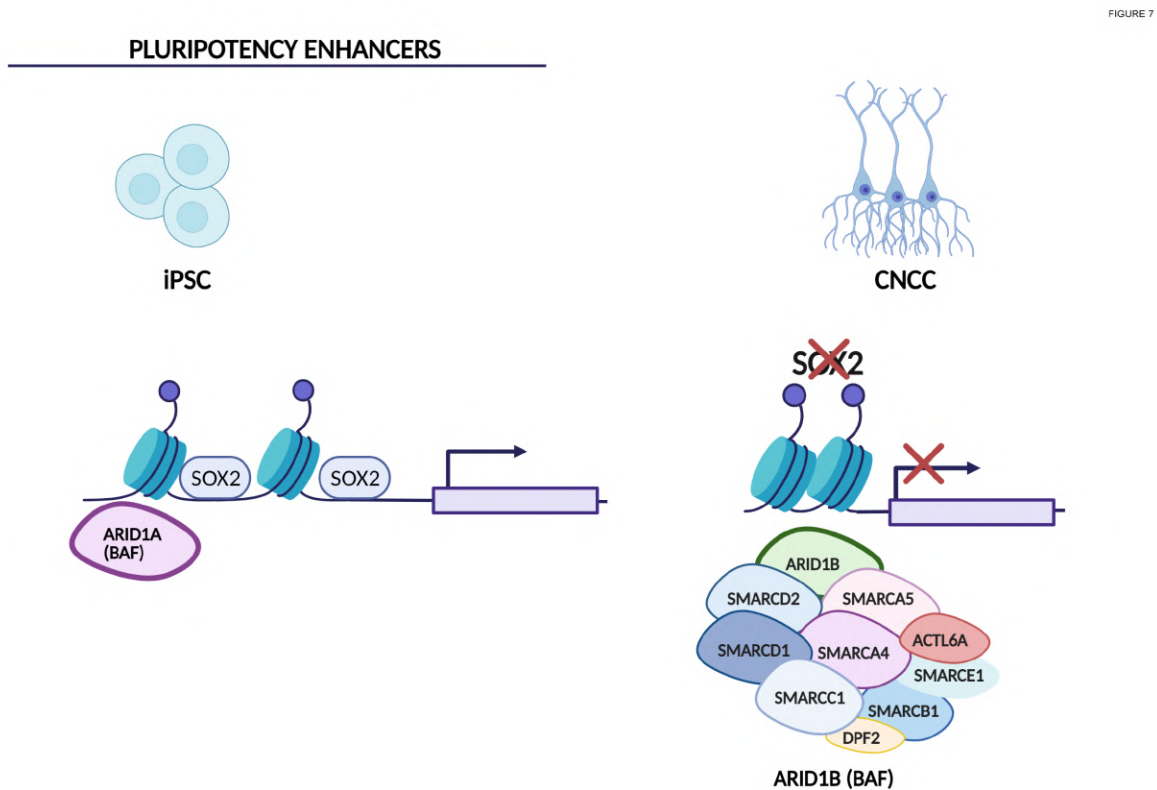
544 Pluripotency is orchestrated by a transcription factor network that needs to be extinguished in an orderly
545 manner to enable lineage commitment and differentiation⁵²⁻⁵⁴. We find that ARID1B-BAF plays an
546 essential role in this process, by means of a repressive activity at the pluripotency enhancers of the SOX2
547 and NANOG networks. Similarly, an association between SOX3 and the SMARCA2 ATPase subunit of BAF
548 was recently suggested in a study of neural development in the Nicolaides-Baraitser syndrome⁵⁵. It is
549 worth noting that Coffin-Siris and Nicolaides-Baraitser syndromes share many physical and neurological
550 phenotypes⁵⁵⁻⁵⁷.

551 The BAF complex is predominantly considered as a transcriptional activator, which balances out the
552 Polycomb Repressor Complexes (PRC1, PRC2) in the modulation of gene expression^{7,58}. Nonetheless,
553 repressing activity for BAF was also reported. For instance, a study conducted on hepatocellular
554 carcinoma cell lines uncovered that ARID1A-containing BAF activates and represses roughly equal
555 numbers of genes, while ARID1B-containing BAF was found to primarily repress enhancer activity⁴⁷. Our
556 experiments corroborate these findings, supporting an enhancer-repressor function for ARID1B-BAF. We
557 demonstrate that the repressive activity of ARID1B-BAF is specific to a set of ~4,900 enhancers and ~600
558 promoters, enriched for the SOX2 and NANOG binding sites. In *ARID1B*-wt conditions, these cis-regulatory
559 elements are highly active at the iPSC stage, moderately active in the first four days of neural crest
560 differentiation, and finally repressed by the day-5, a time point in which we reported the peak of ARID1B
561 protein expression. The patient cells exhibit aberrant chromatin accessibility at these cis-regulatory
562 elements for many days after the onset of differentiation, enforcing a long-lasting pluripotency signature
563 which persists even after two weeks of differentiation.

564 Patient-26 derived cells display the most extreme cellular and molecular phenotype, with ~20% of the
565 cells remaining pluripotent at the day-14 of differentiation, likely as a consequence of higher *SOX2* and
566 *NANOG* expression and activity. The cells derived from this patient also show the highest levels of ARID1A
567 binding at these enhancers at the day-5 of CNCC differentiation. Although it is difficult to formally
568 compare disease severity since there are no accepted severity scales for Coffin-Siris syndrome, it is worth
569 noting that Patient-26 presents clinically more severe than Patient-19. For example, Patient-26 was not
570 able to speak at 7 years, whilst Patient-19 started speaking at 4 years. Additionally, the Patient-26 is
571 affected by pyloric stenosis, a congenital anomaly in the digestive system thought to be associated with
572 impaired migration of the enteric neural crest. We consider it unlikely that the difference is caused solely
573 by the mutations in *ARID1B*, since both patients show comparable reduction in ARID1B protein levels. We
574 speculate that additional genetic factors may concur with *ARID1B* haploinsufficiency to determine the
575 clinical severity of the syndrome. Nonetheless, these lines of evidence potentially establish a direct
576 correlation between reduced attenuation of pluripotency enhancers, inefficient exit from pluripotency,
577 impaired cell differentiation, and disease severity (Fig. 7). However, additional experiments with a larger
578 set of patient-derived cell lines would be required to support this model. Furthermore, it would also be
579 important to investigate other differentiation lineages to elucidate whether the ARID1A/ARID1B switch is
580 limited to the neural crest differentiation or if instead it represents a more widespread mechanism utilized
581 by stem cells to exit the pluripotent state and undergo lineage commitment.

582 Finally, further investigations will be necessary to elucidate the mechanism(s) responsible for the
583 repressive activity of ARID1B-BAF. Recent studies have demonstrated that the function of BAF (including
584 ARID1A-BAF) as transcriptional activator is mediated by the AP-1 transcription factors^{55,59,60}. On the other
585 hand, little is known of potential co-factors mediating the repressive function of ARID1B-BAF. The

586 hypothesis that SALL4 might be mediating such repressive activity is fascinating and it opens up new
587 research directions.
588



589
590

591 **Figure 7 – A novel role for the ARID1B-BAF in the regulation of the exit from pluripotency.** In iPSCs, the
592 pluripotency enhancers are maintained in active state by the ARID1A-BAF. When the neural crest
593 differentiation is induced, ARID1B-BAF replaces ARID1A-BAF at these enhancers, eliciting their
594 attenuation. The *ARID1B* haploinsufficient cells fail to perform the ARID1A/ARID1B switch, and maintain
595 ARID1A-BAF at the pluripotency enhancers throughout the differentiation. Consequently, these
596 enhancers remain aberrantly active and bound by SOX2 and NANOG for several days along the
597 differentiation process. As a consequence, the gene network responsible for the exit from pluripotency
598 is not efficiently activated and the CNCC differentiation is impaired.

599

600 Acknowledgements

601 The authors are deeply grateful to the patients and their families, who donated the samples for this
602 research. The authors thank the physicians and technicians who collected and cultured the skin
603 samples. This work was funded by the G. Harold and Leila Y. Mathers Foundation (MT), and the Gisela
604 Thier Fellowship (GWES). The authors thank the Genomic Facilities at Thomas Jefferson University and at
605 the Wistar Institute for the sequencing effort. The authors are grateful to Kelly Vonk (Leiden University)
606 for the help with experimental procedures in the iPSC generation. An invaluable support was provided to
607 the authors by the Stem Cell and Regenerative Neuroscience Center at Thomas Jefferson University, and
608 in particular by Dr. Elizabeth Kropf. Lastly, MT and GWES are thankful to Dr. Samantha Vergano (Children's
609 Hospital of the King Daughters) for making this collaboration and this work possible.

610

611 **Author contributions:** MT, GWES and LP designed the project. GWES recruited the patients and obtained
612 the skin fibroblasts. HMMM and CF reprogrammed the patient fibroblasts into iPSCs and assessed their
613 quality. LD performed initial iPSC characterization experiments. LP performed most of the experiments.
614 PP, ATC, CAO, and SAW contributed to specific experiments (flowcytometry, immunoblots, mass-
615 spectrometry). BC provided intellectual contribution and financial support to PP. MT, LP and SD analyzed
616 the data. MT, GWES, and LP wrote the manuscript, which was read and approved by all the authors.

617 **Data availability:** The original genome-wide data generate for this paper are deposited in the GEO
618 database (accession number GSE169654).

619

620 **MATERIALS AND METHODS**

621

622 **Human iPSC culture**

623 Control iPSC lines were obtained from the iPSC Core of the University of Pennsylvania (Control line-1: SV20
624 line, male, age 43) and from the Coriell Institute for Medical Research (Camden, NJ. Control line-2:
625 GM23716, female, age 16).

626 Skin fibroblasts from the two pediatric Coffin-Siris patients (one teenager one young adult) were obtained
627 by the team of Dr. Gijs Santen at Leiden University. Patient 19 is a female, while Patient 26 is a male. The
628 fibroblasts were reprogrammed into iPSCs with the polycistronic lentiviral vector
629 LV.RRL.PPT.SF.hOKSM.idTomato.-preFRT by LUMC human iPSC Hotel as described elsewhere^{61,62}.

630 Multiple clones per line were derived. For each clone, pluripotency was assessed by immunofluorescence
631 microscopy using antibodies against NANOG, OCT3/4, SSEA4 and Tra-1-81 under maintenance conditions
632 and antibodies against (TUBB3, AFP and CD31) after spontaneous differentiation into the 3 germ layers as
633 described elsewhere⁶¹. Clones with proper pluripotent characteristics were selected for downstream
634 usage. Karyotyping by G binding was assessed for all the four lines by the Leiden University Medical Center
635 and Short Tandem Repeat (STR) profiling was performed by the Leiden University Medical Center and and
636 then replicated by the Stem Cell and Regenerative Neuroscience Center at Thomas Jefferson University.
637 The iPSC lines were expanded in feeder-free, serum-free mTeSR™1 medium (STEMCELL Technologies).
638 Cells were passaged ~1:10 at 80% confluency using ReLeSR (STEMCELL Technologies) and small cell
639 clusters (50–200 cells) were subsequently plated on tissue culture dishes coated overnight with Geltrex™
640 LDEV-Free hESC-qualified Reduced Growth Factor Basement Membrane Matrix (Fisher-Scientific).

641

642 **CNCC Differentiation**

643 The iPSC lines were differentiated into CNCC as previously described²⁸. Briefly, iPSCs were treated with
644 CNCC Derivation media: 1:1 Neurobasal medium/D-MEM F-12 medium (Invitrogen), 0.5× B-27
645 supplement with Vitamin A (50× stock, Invitrogen), 0.5× N-2 supplement (100× stock, Invitrogen), 20
646 ng/ml bFGF (Biolegend), 20 ng/ml EGF (Sigma-Aldrich), 5 µg/ml bovine insulin (Sigma-Aldrich) and 1×
647 Glutamax-I supplement (100× stock, Invitrogen). Medium (3ml) was changed every day. Three days after
648 the appearance of the migratory CNCC, cells were detached using accutase and placed into geltrex-coated
649 plates. The early migratory CNCCs were then transitioned to CNCC early maintenance media: 1:1
650 Neurobasal medium/D-MEM F-12 medium (Invitrogen), 0.5× B-27 supplement with Vitamin A (50× stock,
651 Invitrogen), 0.5× N-2 supplement (100× stock, Invitrogen), 20 ng/ml bFGF (Biolegend), 20 ng/ml EGF
652 (Sigma-Aldrich), 1 mg/ml bovine serum albumin, serum replacement grade (Gemini Bio-Products # 700-
653 104P) and 1× Glutamax-I supplement (100× stock, Invitrogen).

654

655

656 **ARID1B Knock-down**

657 To make concentrated lentivirus, HEK293T cells were transfected with a pLenti plasmid in which we cloned
658 an shRNA for *ARID1B* (GPP Web Portal: TRCN0000107361). iPSCs were lentivirally transduced by
659 incubating the cells with concentrated virus overnight at 37 C. The next morning the media was changed,
660 and 2 mg/ml puromycin (InvivoGen) were added 24h after infection. After 72 hours, the iPSCs that
661 survived the selection were then differentiated in CNCC using the above described protocol, and collected
662 at Day-5 for the genomic experiments. The cells were kept under puromycin selection for the entire
663 duration of the differentiation. The knock-down efficiency was quantified via western blot.
664

665 **Flow cytometry analysis of surface markers**

666 To obtain a single cell suspension for flow cytometry analysis, control and patient cells were treated with
667 Accutase for 5 minutes. Cells were then washed with cold PBS-2% FBS and live cells were counted. 1×10^6
668 cells/condition were resuspended in 100 μ L PBS-2% FBS and stained. For pluripotency evaluation, 4 μ L of
669 the respective antibodies were used: APC anti-human SSEA-4 antibody (Biolegend, #330417) and PE anti-
670 human TRA-1-60-R antibody (Biolegend, #330609). For analysis of differentiation, 2 μ L of the respective
671 antibodies were used: FITC anti-human CD10 (Miltenyi Biotec, #130-124-262) and APC anti-human CD99
672 (Miltenyi Biotec, #130-121-096). Cells were incubated for 15 min on ice and protected from light, before
673 transferring them into FACS tubes containing additional 300 μ L PBS-2% FBS. Flow cytometry data were
674 acquired using a BD LSR II flow cytometer and analyzed with FlowJo Software version 10.7.
675

676 **Western Blot**

677 For total lysate, cells were harvested and washed three times in 1X PBS and lysed in RIPA buffer (50mM
678 Tris-HCl pH7.5, 150mM NaCl, 1% Igepal, 0.5% sodium deoxycholate, 0.1% SDS, 500uM DTT) with proteases
679 inhibitors. Twenty μ g of whole cell lysate were loaded in Novex WedgeWell 4-20% Tris-Glycine Gel
680 (Invitrogen) and separated through gel electrophoresis (SDS-PAGE) Tris-Glycine-SDS buffer (Invitrogen).
681 The proteins were then transferred to ImmunBlot PVDF membranes (ThermoFisher) for antibody probing.
682 Membranes were incubated with 10% BSA in TBST for 30 minutes at room temperature (RT), then
683 incubated for variable times with the suitable antibodies diluted in 5% BSA in 1X TBST, washed with TBST
684 and incubated with a dilution of 1:10000 of secondary antibody for one hour at RT. The antibody was then
685 visualized using Super Signal West Dura Extended Duration Substrat (ThermoFisher) and imaged with
686 Amersham Imager 680.
687

688 **Cell fractionation**

689 5×10^6 cells/condition were collected and suspended in E1 buffer (50mM HEPES-KOH, 140mM NaCl, 1mM
690 EDTA, 10% glycerol, 0.5% NP-40, 0.25% Triton X-100, 1mM DTT, 1X Proteinase Inhibitor) followed by a
691 centrifugation step of 1100 g at 4°C for 2min. The cytoplasmic fraction was collected in a fresh tube. Cells
692 were washed two more times with E1 buffer. Pellet was subsequently suspended in E2 buffer (10mM Tris-
693 HCl, 200mM NaCl, 1mM EDTA, 0.5mM EGTA, 1X Proteinase Inhibitor) followed by a centrifugation step of
694 1100 g at 4°C for 2 min. Nuclear fraction was collected in a fresh tube. Cells were washed two more times
695 with E2 buffer. After the third wash, pellet was suspended in E3 buffer (500mM Tris-HCl, 500mM NaCl, 1X
696 Proteinase Inhibitor) and sonicated for 15 sec (5 sec ON/ 5 sec OFF). Cytoplasmic, nuclear and chromatin
697 fraction were centrifuge at 16000 g for 10min at 4°C.
698

699 **Antibodies**

700 ARID1B ChIP-Seq: Abcam ab57461. ARID1B western blot: Santa-Cruz sc-32762 and Abcam ab57461.
701 ARID1A ChIP-Seq: GeneTex GTX129433. ARID1A western blot: Cell Signaling Technologies 12354S. Beta-
702 Actin western blot: Cell Signaling Technologies 8457P. SOX2 ChIP-Seq: Active Motif 39843. NANOG ChIP-
703 Seq: R&D Systems AF1997. H3K27ac ChIP-Seq: Abcam ab4729. GAPDH western blot: Cell Signaling
704 Technologies 5174T. CD10 Flow Cytometry: Miltenyi Biotec 130-124-262. CD99 Flow Cytometry: Miltenyi

705 Biotech 130-121-086. SSEA4 Flow Cytometry: Biologend 330417. TRA-1-60-R Flow Cytometry: Biologend
706 330609. IgG ChIP-qPCR: Cell Signaling Technologies 2729S. Cell Signaling HRP-conjugated anti-rabbit
707 (7074S) and anti-mouse (7076S) were used as secondary antibodies in western blot. Spike-in Antibody:
708 Active Motif 61686. Spike-in Chromatin: Active Motif 53083.

709

710 **Real-time quantitative polymerase chain reaction (RT-qPCR)**

711 Cells were lysed in Tri-reagent and RNA was extracted using the Direct-zol RNA MiniPrep kit (Zymo
712 research). 600ng of template RNA was retrotranscribed into cDNA using RevertAid first strand cDNA
713 synthesis kit (Thermo Scientific) according to manufacturer directions. 15ng of cDNA were used for each
714 real-time quantitative PCR reaction with 0.1 μ M of each primer, 10 μ L of PowerUp™ SYBR™ Green Master
715 Mix (Applied Biosystems) in a final volume of 20 μ L, using QuantStudio 3 Real-Time PCR System (Applied
716 Biosystem). Thermal cycling parameters were set as following: 3 minutes at 95°C, followed by 40 cycles of
717 10 s at 95°C, 20 s at 63°C followed by 30 s at 72°C. Each sample was run in triplicate. 18S rRNA was used
718 as normalizer. Primer sequences are reported in Supplementary Table S1.

719

720 **ChIP-Seq and ChIP-qPCR**

721 Samples from different conditions were processed together to prevent batch effects.

722 For SOX2, NANOG and H3K27ac, for each replicate, 10 million cells were cross-linked with 1%
723 formaldehyde for 5 min at room temperature, quenched with 125mM glycine, harvested and washed
724 twice with 1 \times PBS. The pellet was resuspended in ChIP lysis buffer (150 mM NaCl, 1% Triton X-100, 0.7%
725 SDS, 500 μ M DTT, 10 mM Tris-HCl, 5 mM EDTA) and chromatin was sheared to an average length of 200–
726 500 bp, using a Covaris S220 Ultrasonicator. The chromatin lysate was diluted with SDS-free ChIP lysis
727 buffer. For ChIP-seq, 10 μ g of antibody (3 μ g for H3K27ac) was added to 5 μ g of sonicated chromatin along
728 with Dynabeads Protein A magnetic beads (Invitrogen) and incubated at 4 °C overnight. For SOX2 and
729 NANOG ChIP-seq, 10 ng of spike-in Drosophila chromatin (Active Motif) was added to each sample with
730 2 μ g spike-in antibody (Active Motif). On day 2, beads were washed twice with each of the following
731 buffers: Mixed Micelle Buffer (150 mM NaCl, 1% Triton X-100, 0.2% SDS, 20 mM Tris-HCl, 5 mM EDTA,
732 65% sucrose), Buffer 500 (500 mM NaCl, 1% Triton X-100, 0.1% Na deoxycholate, 25 mM HEPES, 10 mM
733 Tris-HCl, 1 mM EDTA), LiCl/detergent wash (250 mM LiCl, 0.5% Na deoxycholate, 0.5% NP-40, 10 mM Tris-
734 HCl, 1 mM EDTA) and a final wash was performed with 1 \times TE. Finally, beads were resuspended in 1 \times TE
735 containing 1% SDS and incubated at 65 °C for 10 min to elute immunocomplexes. Elution was repeated
736 twice, and the samples were further incubated overnight at 65 °C to reverse cross-linking, along with the
737 untreated input (5% of the starting material). On day 3, after treatment with 0.5 mg/ml Proteinase K for
738 1h at 65 °C, DNA was purified with Zymo ChIP DNA Clear Concentrator kit and quantified with QUBIT.

739 For ARID1A and ARID1B ChIP-Seq, 10 million cells were cross-linked with EGS (150 mM) for 30min at room
740 temperature followed by a second cross-link with 1% formaldehyde for 15 min at room temperature. The
741 formaldehyde was quenched with by adding glycine (0.125M) for 10 min at room temperature. Cells were
742 washed twice with 1 \times PBS. Pellet was resuspended in buffer LB1 (50 mM Hepes-KOH, 140 mM NaCl, 1 mM
743 EDTA, 10% Glycerol, 0.5% NP-40, 0.255 Triton X-100), incubated 10 min at 4 °C followed by a
744 centrifugation step of 600g for 5 min at 4 °C. Pellet was suspended in buffer LB2 (10 mM Tris-HCl, 20 mM
745 NaCl, 1 mM EDTA, 0.5 mM EGTA) incubated 10 min at 4 °C followed by a centrifugation step of 600g for 5
746 min at 4 °C. Cells were then resuspended in buffer LB3 (10 mM Tris-HCl, 200 mM NaCl, 1mM EDTA, 0.5
747 mM EGTA, 0.1% Na-DOC, 0.5% N-lauroylsarcosine) incubated 10 min at 4 °C followed by a centrifugation
748 step of 600g for 5min at 4 °C. Pellet was suspended in LB3 and chromatin was sheared to an average
749 length of 200–500 bp, using a Covaris S220 Ultrasonicator. For each sample, 15 μ g of sonicated chromatin
750 was incubated at 4 °C overnight along with Dynabeads Protein G conjugated with 10 μ g of antibody. On
751 day 2, beads were washed once with each of the following buffers: WB1 (50 mM Tris-HCl, 150 mM NaCl,
752 0.15 SDS, 0.1% Na-DOC, 1% Triton X-100, 1 mM EDTA), WB2 (50 mM Tris-HCl, 500 mM NaCl, 0.15 SDS,

753 0.1% Na-DOC, 1% Triton X-100, 1 mM EDTA), WB3 (10 mM Tris-HCl, 250 mM LiCl, 0.55 NP-40. 0.55 Na-
754 DOC, 1 mM EDTA), TE Buffer (10 mM Tris-HCl, 1mM EDTA). Finally, beads were resuspended in EB (10 mM
755 tris-HCl, 0.55 SDS, 300 mM NaCl, 5mM EDTA) and incubated at 65 °C for 30 min to elute
756 immunocomplexes. Elution was repeated twice, and the samples were further incubated overnight at 65
757 °C to reverse cross-linking, along with the untreated input (5% of the starting material). On day 3, after
758 treatment with 0.5 mg/ml Proteinase K for 1h at 65 °C.

759 For all ChIP-seq experiments, barcoded libraries were made with NEB ULTRA II DNA Library Prep Kit for
760 Illumina, and sequenced on Illumina NextSeq 500, producing 75bp SE reads.

761 For ChIP-qPCR, on day 1 the sonicated lysate was aliquot into single immunoprecipitations of 2.5×10^6
762 cells each. A specific antibody or a total rabbit IgG control was added to the lysate along with Protein A
763 magnetic beads (Invitrogen) and incubated at 4 °C overnight. On day3, ChIP eluates and input were
764 assayed by real-time quantitative PCR in a 20 µl reaction with the following: 0.4 µM of each primer, 10 µl
765 of PowerUp SYBR Green (Applied Biosystems), and 5 µl of template DNA (corresponding to 1/40 of the
766 elution material) using the fast program on QuantStudio qPCR machine (Applied Biosystems). Thermal
767 cycling parameters were: 20sec at 95 °C, followed by 40 cycles of 1sec at 95°C, 20sec at 60°C.

768

769 **ChIP-seq Analyses**

770 After removing the adapters, the sequences were aligned to the reference hg19, using Burrows Wheeler
771 Alignment tool (BWA), with the MEM algorithm⁶³. Aligned reads were filtered based on mapping quality
772 (MAPQ > 10) to restrict our analysis to higher quality and likely uniquely mapped reads, and PCR duplicates
773 were removed. We called peaks for each individual using MACS2⁶⁴ (H3K27ac) or Homer⁶⁵, at 5% FDR, with
774 default parameters.

775

776 **RNA-Seq**

777 Cells were lysed in Tri-reagent (Zymo research) and total RNA was extracted using Quick-RNA Miniprep
778 kit (Zymo research) according to the manufacturer's instructions. RNA was further quantified using
779 DeNovix DS-11 Spectrophotometer while the RNA integrity was checked on Bioanalyzer 2100 (Agilent).
780 Only samples with RIN value above 8.0 were used for transcriptome analysis. RNA libraries were prepared
781 using 1 µg of total RNA input using NEBNext[®] Poly(A) mRNA Magnetic Isolation Module, NEBNext[®]
782 UltraTM II Directional RNA Library Prep Kit for Illumina[®] and NEBNext[®] UltraTM II DNA Library Prep Kit for
783 Illumina[®] according to the manufacturer's instructions (New England Biolabs).

784

785 **RNA-Seq Analyses**

786 Reads were aligned to hg19 using STAR v2.5⁶⁶, in 2-pass mode with the following parameters: --
787 quantMode TranscriptomeSAM --outFilterMultimapNmax 10 - -outFilterMismatchNmax 10 --
788 outFilterMismatchNoverLmax 0.3 --alignIntronMin 21 -- alignIntronMax 0 --alignMatesGapMax 0 --
789 alignSJoverhangMin 5 --runThreadN 12 -- twopassMode Basic --twopass1readsN 60000000 --
790 sjdbOverhang 100. We filtered bam files based on alignment quality (q = 10) using Samtools v0.1.19⁶³. We
791 used the latest annotations obtained from Ensembl to build reference indexes for the STAR alignment.
792 Kallisto⁶⁷ was used to count reads mapping to each gene. RSEM⁶⁸ was instead used to obtain FPKM
793 (Fragments Per Kilobase of exon per Million fragments mapped). We analyzed differential gene expression
794 levels with DESeq2⁶⁹, with the following model: design = ~condition, where condition indicates either CTRL
795 or Patients.

796

797 **ATAC-Seq**

798 For ATAC-Seq experiments, 50,000 cells per condition were processed as described in the original ATAC-
799 seq protocol paper⁷⁰. ATAC-seq data were processed with the same pipeline described for ChIP-seq, with
800 one modification: all mapped reads were offset by +4 bp for the forward-strand and -5 bp for the reverse-

801 strand. After peak calling (MACS2), peaks replicated in all 4 lines (hereafter consensus peaks) were used
802 for downstream analyses.

803

804 **Nuclear extract, IP and LC-MS/MS**

805 After collection, cells were washed twice with ice cold PBS before resuspension in co-IP buffer (20mM Tris
806 pH 7.9, 100mM NaCl, 0.1% NP-40, 0.5mM DTT, protease inhibitors), and rotated for 5 minutes at 4°C.
807 After spinning down at 2000rpm for 10 minutes, the nuclear pellet was resuspended in buffer C (20mM
808 Tris pH 8.0, 1.5mM MgCl₂, 0.42M NaCl, 25% glycerol, 0.2mM EDTA, 0.5mM DTT, protease inhibitors),
809 dounce homogenized (with B pestle), and incubated at 4°C for 30 minutes. The extract was centrifuged at
810 12,000rpm for 30 minutes, and the supernatant was kept as nuclear extract. The nuclear extract was
811 dialyzed overnight in BC80 (20mM Tris pH 8.0, 80mM KCl, 0.2mM EDTA, 10% glycerol, 1mM B-
812 mercaptoethanol, 0.2mM phenylmethylsulfonyl fluoride (PMSF)), cleared, and stored at -80°C. For the IP,
813 1.5mg of nuclear extract was incubated for 3 hours at 4°C with 6µg ARID1B antibody and 50µL of
814 Dynabeads Protein A, and the control IP was performed with 0.75mg of nuclear extract and 25µL of
815 Dynabeads Protein A. Beads were washed three times with co-IP buffer, followed by a final wash with
816 0.05% NP-40 in PBS. Elution was performed by agitation in 0.1M glycine pH 3.0 for one minute, and 1M
817 Tris base pH 11.0 was added to neutralize the pH of the eluate. Eluates were prepared for SDS-PAGE and
818 run on a Novex WedgeWell 10% Tris-Glycine Gel (Invitrogen) with Tris-Glycine-SDS buffer (Bio-Rad), at
819 110V for 10 minutes. The gel was stained with Colloidal Blue staining kit (Invitrogen), and further
820 processed at the proteomics facility at the Wistar Institute. Briefly, the gel lanes were excised, reduced
821 with TCEP, alkylated with iodoacetamide, and digested with trypsin. Tryptic digests were analyzed using
822 LC-MS/MS (a standard 90 minute LC gradient on the Thermo Q Exactive HF mass spectrometer). MS/MS
823 spectra were searched with full tryptic specificity against the UniProt human database (10/02/2020) using
824 MaxQuant 1.6.17.0, and also searched for the common protein N-terminal acetylation, Asn deamidation,
825 and Met oxidation. Protein and peptide false discovery rate was set at 1%.

826

827 **Statistical and genomic analyses**

828 All statistical analyses were performed using R v3.3.1. BEDtools v2.27.1⁷¹ was used for genomic analyses.
829 Pathway analysis was performed with Ingenuity Pathway Analysis Suite (QIAGEN Inc.,
830 <https://www.qiagenbioinformatics.com/products/ingenuity-pathway-analysis>). Motif analyses were
831 performed using the Meme-Suite⁷², and specifically with the Meme-ChIP application. Fasta files of the
832 regions of interest were produced using BEDTools v2.27.1. Shuffled input sequences were used as
833 background. E-values < 0.001 were used as threshold for significance⁷².

834

835

836 **References**

- 837 1. Wang, W. *et al.* Purification and biochemical heterogeneity of the mammalian SWI-SNF
838 complex. *EMBO J* **15**, 5370-82 (1996).
- 839 2. Braun, S.M.G. *et al.* BAF subunit switching regulates chromatin accessibility to control cell
840 cycle exit in the developing mammalian cortex. *Genes Dev* **35**, 335-353 (2021).
- 841 3. Lessard, J. *et al.* An essential switch in subunit composition of a chromatin remodeling
842 complex during neural development. *Neuron* **55**, 201-15 (2007).
- 843 4. Gatchalian, J. *et al.* A non-canonical BRD9-containing BAF chromatin remodeling complex
844 regulates naive pluripotency in mouse embryonic stem cells. *Nat Commun* **9**, 5139 (2018).

- 845 5. Ho, L. *et al.* An embryonic stem cell chromatin remodeling complex, esBAF, is an essential
846 component of the core pluripotency transcriptional network. *Proc Natl Acad Sci U S A* **106**,
847 5187-91 (2009).
- 848 6. Ho, L. *et al.* An embryonic stem cell chromatin remodeling complex, esBAF, is essential
849 for embryonic stem cell self-renewal and pluripotency. *Proc Natl Acad Sci U S A* **106**, 5181-
850 6 (2009).
- 851 7. Alfert, A., Moreno, N. & Kerl, K. The BAF complex in development and disease. *Epigenetics*
852 *Chromatin* **12**, 19 (2019).
- 853 8. Halgren, C. *et al.* Corpus callosum abnormalities, intellectual disability, speech
854 impairment, and autism in patients with haploinsufficiency of ARID1B. *Clin Genet* **82**, 248-
855 55 (2012).
- 856 9. Hoyer, J. *et al.* Haploinsufficiency of ARID1B, a member of the SWI/SNF-a chromatin-
857 remodeling complex, is a frequent cause of intellectual disability. *Am J Hum Genet* **90**,
858 565-72 (2012).
- 859 10. Santen, G.W. *et al.* Mutations in SWI/SNF chromatin remodeling complex gene ARID1B
860 cause Coffin-Siris syndrome. *Nat Genet* **44**, 379-80 (2012).
- 861 11. Tsurusaki, Y. *et al.* Coffin-Siris syndrome is a SWI/SNF complex disorder. *Clin Genet* **85**,
862 548-54 (2014).
- 863 12. van der Sluijs, P.J. *et al.* The ARID1B spectrum in 143 patients: from nonsyndromic
864 intellectual disability to Coffin-Siris syndrome. *Genet Med* **21**, 1295-1307 (2019).
- 865 13. Vergano, S.A., van der Sluijs, P.J. & Santen, G. ARID1B-Related Disorder. in
866 *GeneReviews((R))* (eds. Adam, M.P. *et al.*) (Seattle (WA), 1993).
- 867 14. Santen, G.W. *et al.* Coffin-Siris syndrome and the BAF complex: genotype-phenotype
868 study in 63 patients. *Hum Mutat* **34**, 1519-28 (2013).
- 869 15. Wiczorek, D. *et al.* A comprehensive molecular study on Coffin-Siris and Nicolaides-
870 Baraitser syndromes identifies a broad molecular and clinical spectrum converging on
871 altered chromatin remodeling. *Hum Mol Genet* **22**, 5121-35 (2013).
- 872 16. Wright, C.F. *et al.* Genetic diagnosis of developmental disorders in the DDD study: a
873 scalable analysis of genome-wide research data. *Lancet* **385**, 1305-14 (2015).
- 874 17. Jung, E.M. *et al.* Arid1b haploinsufficiency disrupts cortical interneuron development and
875 mouse behavior. *Nat Neurosci* **20**, 1694-1707 (2017).
- 876 18. Ka, M., Chopra, D.A., Dravid, S.M. & Kim, W.Y. Essential Roles for ARID1B in Dendritic
877 Arborization and Spine Morphology of Developing Pyramidal Neurons. *J Neurosci* **36**,
878 2723-42 (2016).
- 879 19. Shibutani, M. *et al.* Arid1b Haploinsufficiency Causes Abnormal Brain Gene Expression
880 and Autism-Related Behaviors in Mice. *Int J Mol Sci* **18**(2017).
- 881 20. Smith, A.L., Jung, E.M., Jeon, B.T. & Kim, W.Y. Arid1b haploinsufficiency in parvalbumin-
882 or somatostatin-expressing interneurons leads to distinct ASD-like and ID-like behavior.
883 *Sci Rep* **10**, 7834 (2020).
- 884 21. Sausen, M. *et al.* Integrated genomic analyses identify ARID1A and ARID1B alterations in
885 the childhood cancer neuroblastoma. *Nat Genet* **45**, 12-7 (2013).
- 886 22. Lu, J. *et al.* Stem cell factor SALL4 represses the transcriptions of PTEN and SALL1 through
887 an epigenetic repressor complex. *PLoS One* **4**, e5577 (2009).

- 888 23. Miller, A. *et al.* Sall4 controls differentiation of pluripotent cells independently of the
889 Nucleosome Remodelling and Deacetylation (NuRD) complex. *Development* **143**, 3074-84
890 (2016).
- 891 24. Tatetsu, H. *et al.* SALL4, the missing link between stem cells, development and cancer.
892 *Gene* **584**, 111-9 (2016).
- 893 25. Yang, J. *et al.* Genome-wide analysis reveals Sall4 to be a major regulator of pluripotency
894 in murine-embryonic stem cells. *Proc Natl Acad Sci U S A* **105**, 19756-61 (2008).
- 895 26. Mashtalir, N. *et al.* Modular Organization and Assembly of SWI/SNF Family Chromatin
896 Remodeling Complexes. *Cell* **175**, 1272-1288 e20 (2018).
- 897 27. Inoue, K. *et al.* Molecular mechanism for distinct neurological phenotypes conveyed by
898 allelic truncating mutations. *Nat Genet* **36**, 361-9 (2004).
- 899 28. Prescott, S.L. *et al.* Enhancer divergence and cis-regulatory evolution in the human and
900 chimp neural crest. *Cell* **163**, 68-83 (2015).
- 901 29. Liu, X. *et al.* De Novo ARID1B mutations cause growth delay associated with aberrant
902 Wnt/beta-catenin signaling. *Hum Mutat* **41**, 1012-1024 (2020).
- 903 30. Vasileiou, G. *et al.* Chromatin-Remodeling-Factor ARID1B Represses Wnt/beta-Catenin
904 Signaling. *Am J Hum Genet* **97**, 445-56 (2015).
- 905 31. Lee, J., Lee, J. & Cho, Y.S. Peroxisome Proliferator-Activated Receptor alpha Agonist and
906 Its Target Nanog Cooperate to Induce Pluripotency. *J Clin Med* **7**(2018).
- 907 32. Mullen, E.M., Gu, P. & Cooney, A.J. Nuclear Receptors in Regulation of Mouse ES Cell
908 Pluripotency and Differentiation. *PPAR Res* **2007**, 61563 (2007).
- 909 33. Rajasingh, J. & Bright, J.J. 15-Deoxy-delta12,14-prostaglandin J2 regulates leukemia
910 inhibitory factor signaling through JAK-STAT pathway in mouse embryonic stem cells. *Exp*
911 *Cell Res* **312**, 2538-46 (2006).
- 912 34. Dodonova, S.O., Zhu, F., Dienemann, C., Taipale, J. & Cramer, P. Nucleosome-bound SOX2
913 and SOX11 structures elucidate pioneer factor function. *Nature* **580**, 669-672 (2020).
- 914 35. King, H.W. & Klose, R.J. The pioneer factor OCT4 requires the chromatin remodeller BRG1
915 to support gene regulatory element function in mouse embryonic stem cells. *Elife*
916 **6**(2017).
- 917 36. Blassberg, R. *et al.* Sox2 levels configure the WNT response of epiblast progenitors
918 responsible for vertebrate body formation. 2020.12.29.424684 (2020).
- 919 37. Bunina, D. *et al.* Genomic Rewiring of SOX2 Chromatin Interaction Network during
920 Differentiation of ESCs to Postmitotic Neurons. *Cell Syst* **10**, 480-494 e8 (2020).
- 921 38. Heurtier, V. *et al.* The molecular logic of Nanog-induced self-renewal in mouse embryonic
922 stem cells. *Nat Commun* **10**, 1109 (2019).
- 923 39. Novo, C.L. *et al.* The pluripotency factor Nanog regulates pericentromeric
924 heterochromatin organization in mouse embryonic stem cells. *Genes Dev* **30**, 1101-15
925 (2016).
- 926 40. De Kumar, B. *et al.* Dynamic regulation of Nanog and stem cell-signaling pathways by
927 Hoxa1 during early neuro-ectodermal differentiation of ES cells. *Proc Natl Acad Sci U S A*
928 **114**, 5838-5845 (2017).
- 929 41. Navarro, P. *et al.* OCT4/SOX2-independent Nanog autorepression modulates
930 heterogeneous Nanog gene expression in mouse ES cells. *EMBO J* **31**, 4547-62 (2012).

- 931 42. Silva, J. *et al.* Nanog is the gateway to the pluripotent ground state. *Cell* **138**, 722-37
932 (2009).
- 933 43. Gagliardi, A. *et al.* A direct physical interaction between Nanog and Sox2 regulates
934 embryonic stem cell self-renewal. *EMBO J* **32**, 2231-47 (2013).
- 935 44. Rodda, D.J. *et al.* Transcriptional regulation of nanog by OCT4 and SOX2. *J Biol Chem* **280**,
936 24731-7 (2005).
- 937 45. Shang, L. *et al.* Mutations in ARID2 are associated with intellectual disabilities.
938 *Neurogenetics* **16**, 307-14 (2015).
- 939 46. Trizzino, M. *et al.* The Tumor Suppressor ARID1A Controls Global Transcription via Pausing
940 of RNA Polymerase II. *Cell Rep* **23**, 3933-3945 (2018).
- 941 47. Raab, J.R., Resnick, S. & Magnuson, T. Genome-Wide Transcriptional Regulation Mediated
942 by Biochemically Distinct SWI/SNF Complexes. *PLoS Genet* **11**, e1005748 (2015).
- 943 48. Pantier, R. *et al.* SALL4 controls cell fate in response to DNA base composition. *Mol Cell*
944 **81**, 845-858 e8 (2021).
- 945 49. Kohlhase, J. SALL4-Related Disorders. in *GeneReviews((R))* (eds. Adam, M.P. *et al.*) (Seattle
946 (WA), 1993).
- 947 50. Pagliaroli, L. & Trizzino, M. The Evolutionary Conserved SWI/SNF Subunits ARID1A and
948 ARID1B Are Key Modulators of Pluripotency and Cell-Fate Determination. *Front Cell Dev*
949 *Biol* **9**, 643361 (2021).
- 950 51. Zhang, Y. *et al.* A switch from hBrm to Brg1 at IFN γ -activated sequences mediates
951 the activation of human genes. *Cell Res* **20**, 1345-60 (2010).
- 952 52. Betschinger, J. *et al.* Exit from pluripotency is gated by intracellular redistribution of the
953 bHLH transcription factor Tfe3. *Cell* **153**, 335-47 (2013).
- 954 53. Jaenisch, R. & Young, R. Stem cells, the molecular circuitry of pluripotency and nuclear
955 reprogramming. *Cell* **132**, 567-82 (2008).
- 956 54. Takahashi, K. & Yamanaka, S. A decade of transcription factor-mediated reprogramming
957 to pluripotency. *Nat Rev Mol Cell Biol* **17**, 183-93 (2016).
- 958 55. Gao, F. *et al.* Heterozygous Mutations in SMARCA2 Reprogram the Enhancer Landscape
959 by Global Retargeting of SMARCA4. *Mol Cell* **75**, 891-904 e7 (2019).
- 960 56. Ejaz, R., Babul-Hirji, R. & Chitayat, D. The evolving features of Nicolaides-Baraitser
961 syndrome - a clinical report of a 20-year follow-up. *Clin Case Rep* **4**, 351-5 (2016).
- 962 57. Wolff, D. *et al.* In-Frame Deletion and Missense Mutations of the C-Terminal Helicase
963 Domain of SMARCA2 in Three Patients with Nicolaides-Baraitser Syndrome. *Mol*
964 *Syndromol* **2**, 237-244 (2012).
- 965 58. Kadoch, C. & Crabtree, G.R. Mammalian SWI/SNF chromatin remodeling complexes and
966 cancer: Mechanistic insights gained from human genomics. *Sci Adv* **1**, e1500447 (2015).
- 967 59. Mathur, R. *et al.* ARID1A loss impairs enhancer-mediated gene regulation and drives colon
968 cancer in mice. *Nat Genet* **49**, 296-302 (2017).
- 969 60. Vierbuchen, T. *et al.* AP-1 Transcription Factors and the BAF Complex Mediate Signal-
970 Dependent Enhancer Selection. *Mol Cell* **68**, 1067-1082 e12 (2017).
- 971 61. Warlich, E. *et al.* Lentiviral vector design and imaging approaches to visualize the early
972 stages of cellular reprogramming. *Mol Ther* **19**, 782-9 (2011).

- 973 62. Chen, J. *et al.* Rational optimization of reprogramming culture conditions for the
974 generation of induced pluripotent stem cells with ultra-high efficiency and fast kinetics.
975 *Cell Res* **21**, 884-94 (2011).
- 976 63. Li, H. *et al.* The Sequence Alignment/Map format and SAMtools. *Bioinformatics* **25**, 2078-
977 9 (2009).
- 978 64. Zhang, Y. *et al.* Model-based analysis of ChIP-Seq (MACS). *Genome Biol* **9**, R137 (2008).
- 979 65. Heinz, S. *et al.* Simple combinations of lineage-determining transcription factors prime
980 cis-regulatory elements required for macrophage and B cell identities. *Mol Cell* **38**, 576-
981 89 (2010).
- 982 66. Dobin, A. *et al.* STAR: ultrafast universal RNA-seq aligner. *Bioinformatics* **29**, 15-21 (2013).
- 983 67. Bray, N.L., Pimentel, H., Melsted, P. & Pachter, L. Near-optimal probabilistic RNA-seq
984 quantification. *Nat Biotechnol* **34**, 525-7 (2016).
- 985 68. Li, B. & Dewey, C.N. RSEM: accurate transcript quantification from RNA-Seq data with or
986 without a reference genome. *BMC Bioinformatics* **12**, 323 (2011).
- 987 69. Love, M.I., Huber, W. & Anders, S. Moderated estimation of fold change and dispersion
988 for RNA-seq data with DESeq2. *Genome Biol* **15**, 550 (2014).
- 989 70. Buenrostro, J.D., Giresi, P.G., Zaba, L.C., Chang, H.Y. & Greenleaf, W.J. Transposition of
990 native chromatin for fast and sensitive epigenomic profiling of open chromatin, DNA-
991 binding proteins and nucleosome position. *Nat Methods* **10**, 1213-8 (2013).
- 992 71. Quinlan, A.R. & Hall, I.M. BEDTools: a flexible suite of utilities for comparing genomic
993 features. *Bioinformatics* **26**, 841-2 (2010).
- 994 72. Bailey, T.L. *et al.* MEME SUITE: tools for motif discovery and searching. *Nucleic Acids Res*
995 **37**, W202-8 (2009).
- 996